



Anti-GBM potential of Rosmarinic acid and its synthetic derivatives via targeting IL17A mediated angiogenesis pathway

Md Shamsuddin Sultan Khan ^{A, C, E}, Mohammad Adnan Iqbal ^B, Muhammad Asif ^A, Tabinda Azam ^B, Majed Al-Mansoub ^A, Rosenani S. M. A. Haque ^B, Mohammed Khadeer Ahamed Basheer ^C, Aman Shah Abdul Majid ^D, Amin Malik Shah Abdul Majid ^{A, C, E*}

Abstract

Glioblastoma (GBM) is a highly angiogenic malignant primary brain tumor with very poor patient survival rates. Here, we present Rosmarinic acid and its new salt and base derivatives that show potential anti-glioblastoma (anti-GBM) activity via disruption of IL17A-mediated downstream angiogenesis pathway. These new compounds were rationally designed, synthesized and the oral CNS physicochemical properties were determined. The anti-GBM activity of the compounds were determined using cell migration and proliferation assays in U87 MG, DBTRG MG and EA.hy926 cells. The compounds activity on IL17A and VEGF expression was determined using ELISA and apoptotic activity was measured by caspase assays. The compounds showed stability in serum and at different pH similar to Rosmarinic acid stoichiometry. Moreover, the salt derivatives were highly hydrophilic and bases were highly lipophilic. These derivatives showed blood-brain barrier permeability >2 fold more than rosmarinic acid ($P < 0.001$). ROS were differentially expressed after treatment with salt and base rosmarinates in U87 MG ($P < 0.0001$). The co

mpounds showed cytostatic and anti-angiogenic activity. The IC_{50} of the silver salts was found to be $> 1200 \mu\text{g/ml}$ thus excluding them from being classed as toxic compounds. In conclusion, metal salts and base rosmarinates demonstrated potent anti-GBM efficacy as IL17A inhibitor with minimal toxicity.

Key Words: IL17A, Chemotherapy, Glioblastoma, Anti-angiogenic activity, Rosmarinic acid, Caffeic acid, Synthetic derivatives

Introduction

Glioblastoma (GBM) is a more highly vascularized and angiogenesis-dependent cancer than other types of cancer. In general, colon and breast cancer treatments can improve the life expectancy of patients but the standard of care (radiotherapy, surgery and chemotherapy) are ineffective in treating GBM. The median survival of GBM is only ~14 months (Stupp et al., 2009). In countries in Southeast Asia such as Malaysia, the National Cancer Council (MAKNA) reported the incidence of brain and nervous system tumor as 3.3 per 100,000 people in 2006 (MAKNA 2006). Current treatment options for patients have remained suboptimal. The field of GBM requires a drug with high target selectivity and minimal toxic effects to other cellular

Significance | Rational drug design approach and the development of rosmarinic acid (RA) and its synthetic derivatives with targeting IL17A might have higher safety profile than traditional chemotherapy.

*Correspondence: Amin Malik Shah Abdul Majid at Department of Pharmacology, School of Pharmaceutical Sciences, Universiti Sains Malaysia, Minden, 11800, Pulau Penang, Malaysia, Tel: +60124230842 Email: aminmalikshah@gmail.com

Edited by Md. Asaduzzaman Shishir, University of Dhaka. And accepted by the Editorial Board April 12, 2019 (received for review December 20, 2018)

Author Affiliation:

^A EMAN Research and Testing Laboratory, School of Pharmaceutical Sciences, Universiti Sains Malaysia, Minden, Pulau Pinang, Malaysia.

^B The School of Chemical Sciences, Universiti Sains Malaysia (USM), 11800 Penang, Malaysia

^C EMAN Biodiscoveries Sdn Bhd, Eureka Complex, Universiti of Science Malaysia, Minden, Penang, Malaysia.

^D Faculty of Medicine, Department of Pharmacology, Quest International University, Ipoh, Perak, Malaysia.

^E EMAN RESEARCH, Level 3, 81 Flushcombe Rd, Blacktown, NSW 2148, Australia

Please cite this article:

Md Shamsuddin Sultan Khan, Mohammad Adnan Iqbal, Muhammad Asif, Tabinda Azam, Majed Al-Mansoub, Rosenani S. M. A. Haque, Mohammed Khadeer Ahamed Basheer, Aman Shah Abdul Majid, Amin Malik Shah Abdul Majid, (2019). Anti-GBM potential of Rosmarinic acid and its synthetic derivatives via targeting IL17A mediated angiogenesis pathway. *Journal of Angiotherapy*, 3(1), 097-122.

systems. In recent years, a number of anti-cancer compounds with anti-angiogenic activity have been derived from medicinal herbs and structurally modified natural compounds. Despite this development, very few drugs that function by disrupting highly expressed pathogenic cytokines are used to treat GBM. For example, the antibody bevacizumab is associated with clinical complications due to off-target antibody interactions. The molecular pathogenesis of cancer provides interesting avenues to develop promising anti-angiogenic agents to treat the GBM. IL17A is highly expressed in human GBM, more so than any other bio-marker. Glioma cells or glioma stem cells express IL17AR, which, upon interaction with IL17A, activates the autocrine and paracrine growth factors (VEGF) and immune cells (Hu et al., 2013). After this molecular activation, glioma-infiltrating immune cells promote increased vascularity and angiogenesis in the GBM at the site of inflammation which further exacerbates the disease (Angelo and Kurzrock, 2007). The chemotherapeutic compounds are ineffective with patients of glioblastoma in particular, for deadly brain tumors. The pro-apoptosis class of chemotherapy termed anti-angiogenic compounds could be potentially used in glioblastoma patient to extend survival rates. These compounds have the ability to disrupt nutrient and oxygen flow to the tumours thus inducing apoptosis of the glioblastoma. Our recent studies showed that anti-angiogenic chemotherapeutic compounds can inhibit blood vessel formation and increase or decrease ROS (reactive oxygen species) production to induce apoptosis of brain tumor cells (Khan et al., 2016). We developed rosmarinic acid and several salt and base derivatives of caffeic acid. This novel development will be an alternative means by which to target IL17A together with the downregulation of HIF1 α (hypoxia inducible factor) and increasing the ROS (reactive oxygen species) to cause apoptosis of glioblastoma cells rather than the current treatment of targeting solely VEGF (vascular endothelial growth factor). The targeting of bio-markers that are highly expressed in cancer cells might be a crucial avenue by which to cure cancer while not affecting normal cells. Drugs with phenolic groups, and carbonyl groups with salt and base nature may have immense therapeutic value for the treatment of metabolic disease such as cancer. The chemotherapeutic compounds that have chelation activity such as cisplatin are life threatening for cancer patients. To lessen the need for such dangerous chemotherapeutic regimens, we developed Rosmarinic acid and also designed salt and base derivatives that show potent anti-angiogenic activity that might be selective and safe to use to treat cancer patient.

Rosmarinic acid (RA) is a widely investigated compound for many diseases which is found at high concentration in plants with the most found in the Lamiaceae family. RA is widely used as antioxidant, anti-inflammatory and anti-microbial activities (Lamaison et al., 1991). RA has potent anti-cancer, anti-lipid peroxidation and apoptotic effect (Sharmila and Manoharan, 2012). RA is effective in preventing COX-2 activation (Scheckel et al., 2008). RA is a type of defensive secondary metabolites in all of these plants. The means by which to synthesize RA and its derivatives such as methyl ester (Petersen et al., 2009; Petersen et al., 2003) has long been sought after. The first synthesis was achieved in 1991 by Albrecht (Talley et al., 1991). The indirect and direct effects of RA on the brain has been previously reported in animal models of Alzheimer's diseases (Fale et al., 2011) and therefore RA could be considered as a potential lead

molecule to design an effective drug for the treatment of malignant brain tumor. To date no study has been conducted to investigate the effect of RA in brain tumors via affecting angiogenesis through dual targeting of interleukin-17A and vascular endothelial growth factor (VEGF). The current study aims to develop a rational anti-glioblastoma agent (RA and its synthetic derivatives) that can act in the CNS, and have the ability to penetrate the blood-brain barrier while having non-toxic effects, anti-resistant properties, prolonged action, drugable efficacy, target specificity to highly expressed cytokines in glioma such as IL17A and be inexpensive to produce. In this endeavor, we have designed and synthesized salt and base derivatives as novel anti-glioblastoma agents. In the current study, RA and its synthetic derivatives were used as potential lead molecule and scaffold backbones which can target IL17A. The biological activity of the compounds was optimized via screening the molecular weight and lipophilic characteristics with inhibitory potential against protein kinase and inflammatory cytokines. Therefore, such rational drug design approach and the development of rosmarinic acid (RA) and its synthetic derivatives with targeting IL17A might have higher safety profile than traditional chemotherapy.

2. Materials and methods

2.1 Designing IL17A antagonists

We have generated many derivatives of RA to inhibit angiogenesis via disruption of IL17A. The computational program NOVA was used to design the derivatives. However, 4 compounds were selected according to the ease of synthesis. These 4 compounds were salts and base derivatives of rosmarinic acid. Sodium rosmarinate (NaR) and silver rosmarinate (AgR) were two salts and diamine caffeate/rosmarinate (FLVM) and imidazole caffeate/rosmarinate (FLVZ) were two bases. All of these compounds were suitable to bind the active pockets of IL17A protein. Additionally, they showed binding to VEGF and p-gp proteins. Despite the lower percentage of homology (13.3%) and similarity (19.7%) (Fig. 1), the active pockets of these two proteins (IL17A and VEGF) could be predicted to be bound by NaR, AgR, FLVM and FLVZ thereby inhibiting angiogenesis or providing anti-angiogenic efficiency.

2.2 Synthesis and Characterization

2.2.1 Chemicals and Reagent

Solvents and chemicals were purchased from Fluka™, Aldrich™, and JT Baker™, USA. Melting points were measured using the Stuart Scientific SMP1 melting point apparatus. UV-Vis spectra were recorded in dimethyl sulfoxide (DMSO) solution with a Perkin Elmer Lambda 25 UV-Vis spectrophotometer. Infrared (IR) spectra were recorded using the Perkin Elmer System 2000 spectrophotometer and the KBr disc method in the range of 4000 to 400 lb pressure at room temperature (RT). ¹H, ¹³C, and nuclear magnetic resonance (NMR) spectra were recorded on a Bruker™ 500 MHz-NMR spectrophotometer relative to N3 and Me in DMSO. Elemental analysis was conducted using a Perkin Elmer™ 2400 Series-11 CHN analyzer. Molar conductivity measurements were carried out using a Jenway™ 4510 conductivity meter and DMSO solvent.

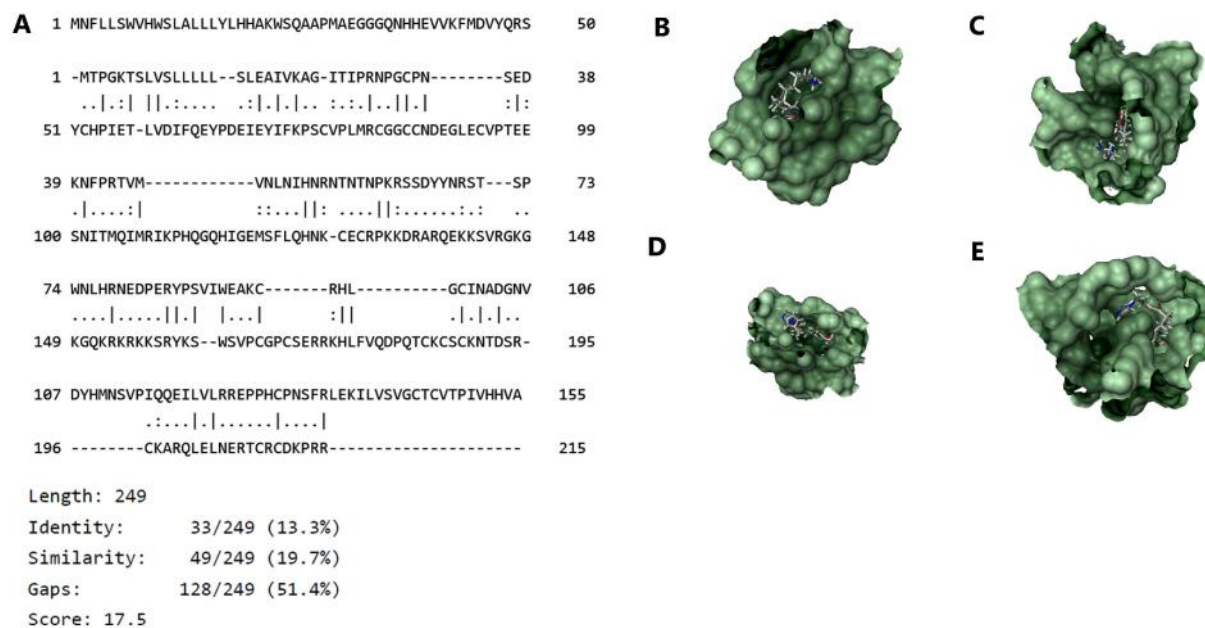


Fig. 1. Alignment of two sequences of IL17A and VEGF and their similarity (A). Fitting of FLVM (B, C) and FLVZ (D, E) with the binding pocket of IL17A (B, D), and VEGF (C, E). Alignment was determined by EMOSS Needle and the binding pocket and binding activity were predicted by the DoGSite Scorer and LEAD IT. NaR and AgR data not shown.

The melting points was measured by the Stuart Scientific SMP1 melting point apparatus. UV-Vis spectra were recorded in DMSO solution with a Perkin Elmer Lambda 25 UV-Vis spectrophotometer. Infrared (IR) spectra were recorded by the Perkin Elmer System 2000 spectrophotometer by using the KBr disc method in the range 4000–400 at room temperature. ¹H, ¹³C NMR spectra were recorded on a Bruker 500 MHz-NMR spectrophotometer relative to SiMe₄ and Me₄Sn in DMSO solvent. Elemental analysis was conducted by the Perkin Elmer 2400 Series-11 CHN analyzer. Molar conductivity measurements were carried out with a Jenway 4510 conductivity meter using a DMSO solvent. A Capillary apparatus was used to determine the melting points of the compounds.

2.2.2 Synthesis of sodium rosmarinate (NaR)

Rosmarinic acid (0.5 g, 1.37 mM) was dissolved in 20 mL 1,4-dioxane (dry). Sodium hydride (NaH) was heated to dry (at 80 °C) for 30 minutes and 6 weight equivalents (0.2 g, 8.32 mM) were added to the Rosemarinic acid solution. The mixture was stirred at room temperature for 30 minutes under an inert atmosphere. The reaction mixture was filtered twice and was washed with fresh 1,4-dioxane (2 × 3 mL). The filtrate was evaporated using rotary evaporator (70 mbar, 60 °C) to obtain a thick yellowish fluid. Diethyl ether (20 mL) was added to the round bottom flask which contained the compound and this was stirred for 5 minutes. Beige colored fluffy precipitates appeared, these were filtered and dried under vacuum. Yield: 0.46 g (72%).

2.2.2(a) Characterization of rosmarinic acid and sodium rosmarinate (NaR)

Rosmarinic acid. FT-IR (KBr, ν cm⁻¹) 1727, 1709, 1645, 1616, 1520, 1463, 1356, 1284, 1459, 1231, 1199, 1152, 1111, 1074, 979, 817. ¹H NMR (500 MHz, DMSO-*d*₆, δ ppm): 9.68, 9.21, 8.83, 8.77, 7.50 (d, *J* = 15 Hz), 7.08, 7.03 (dd, *J* = 8 Hz), 6.80 (d, *J* = 8 Hz), 6.70 (s, 1H),

6.85 (d, *J* = 8Hz, 1H), 6.54 (dd, *J* = 8 Hz, 1H), 6.28 (d, *J* = 16 Hz, 1H), 5.06 (q, 1H), 2.90-3.02 (m, 2H). ¹³C NMR (125.1 MHz, DMSO-*d*₆, δ ppm): 170.8, 165.9, 148.5, 145.9, 145.5, 144.8, 143.9, 127.2, 125.3, 121.6, 120.0, 116.6, 115.7, 115.3, 114.8, 113.2, 72.7, 36.0.

Sodium rosmarinate (NaR). Beige colored fluffy precipitates appeared, were filtered and were dried under vacuum. Yield: 0.46 g (72%). FT-IR (KBr disc): 2857, 2921, 2956 (C-H_{aliph} stretch), 1693 (C=O), 1630 (C=C_{non-arom}), 1602 (C=C_{arom}), 1524, 1446, 1361, 1265 (CH & CH₂ bendings, broad), 1182, 1163, 1116, 1073, 1036, 977. ¹H NMR (500 MHz, DMSO-*d*₆, δ ppm): 9.68, 9.21, 8.83, 8.77, 7.50 (d, *J* = 15 Hz), 7.08, 7.03 (dd, *J* = 8 Hz), 6.80 (d, *J* = 8 Hz), 6.70 (s, 1H), 6.85 (d, *J* = 8Hz, 1H), 6.54 (dd, *J* = 8 Hz, 1H), 6.28 (d, *J* = 16 Hz, 1H), 5.6 (q, 1H), 2.90-3.02 (m, 2H). X-ray was used to confirm the presence of the sodium ion with rosmarinic acid (Fig. 9).

2.2.2 Synthesis of silver rosmarinate (AgR)

Rosmarinic acid (0.5 g, 1.37 mM) and silver acetate (1.36g, 8.22 mM) were mixed in methanol (100 mL) in a round bottom flask. The mixture was stirred at room temperature for 2 days. The reaction mixture was filtered thrice using a pad of celites (Diatomaceous earth Or SiO₂). A Black colored solution was evaporated slowly at room temperature to obtain a black crystalline shiny material.

2.2.2(a) Characterization of silver rosmarinate (AgR)

AgR was recrystallized using diethyl ether and methanol solvent system. Yield: 0.52 g (84%). FT-IR (KBr, ν cm⁻¹) 1696, 1628, 1602, 1520, 1441, 1363, 1256, 1160, 1117, 1074, 977, 853, 813. ¹H NMR (500 MHz, DMSO-*d*₆, δ ppm): 7.45 (d, *J* = 15 Hz), 7.06, 7.00 (d, *J* = 8 Hz), 6.78 (s, 1H), 6.69 (s, 1H), 6.64 (d, *J* = 8 Hz, 1H), 6.53 (d, *J* = 8 Hz, 1H), 6.25 (d, *J* = 16 Hz, 1H), 5.00 (q, 1H), 2.86-3.07 (m, 2H). ¹³C NMR (125.1 MHz, DMSO-*d*₆, δ ppm): 171.5, 166.0, 148.5, 145.6, 145.3, 144.8, 143.8, 128.1, 125.3, 121.3, 119.9, 116.6, 115.8, 115.3, 114.8, E097-E122 | ANGIOTHERAPY | Published online May 11, 2019

113.2, 73.8, 36.4. X-ray was used to confirm the presence of the silver ion with rosmarinic acid (Fig. 9).

2.2.3 Synthesis of FLVM

Flavomin was synthesized by the reaction between caffeic acid and 1,3-diamine (1:1) at 70 °C which was stirred for roughly 48 h using hotplate magnetic stirrer. The resultant product was isolated and filtered using 1,4 dioxane. The filtrate was evaporated and a black yellow product was obtained. The product was sticky and only dissolved in the DMSO. The product was characterized by NMR and FT-IR.

2.2.3(a) Characterization of FLVM

The synthesis of the designed compound was carried out by reacting caffeic acid with 1,3-diamine at 70 °C. ¹H NMR (500 MHz, DMSO-*d*₆, δ, ppm); 1.58 (s, H), 1.84 (qnt, 2H), 2.67 (t, 2H), 3.21 (t, 2H), 6.41 (d, *J* = 7.5 Hz, 1H), 6.62 (d, *J* = 3 Hz, 1H), 6.81 (d, *J* = 3.5 Hz, 1H), 7.12 (s, 1H), 7.36 (d, *J* = 7.5 Hz, 1H), 8.46 (br. s, 1H), 9.28 (br. s, 2H). ¹³C NMR (125.1 MHz, DMSO-*d*₆, δ, ppm); 33.6, 39.4, 41.6, 115.2, 117.4, 120.8, 123.8, 128.9, 141.4, 145.2, 146.1, 171.9. FT-IR (KBr, ν cm⁻¹); 3415 (OH stretch), 3012, 3067 (C-H_{arom}), 2999, 2915 (C-H_{aliph} stretch), 1639 (C=C_{aliph}), 1564 (C=C_{arom}), 1434, 1312 (CH₂ bending).

2.2.4 Synthesis of FLVZ

To prepare the imidazole rosmarinate, 2.0 g (29.3 mM) imidazole was mixed with 1.64 g (29.3 mM) of potassium hydroxide powder in a round bottom flask using DMSO. The solution was stirred and refluxed for 3-4 h at 50 °C. The obtained cloudy material (bromo imidazole) was filtered, evaporated and stored for next steps. To obtain the imidazole rosmarinate, sodium caffeate was prepared using 2g (12 mM) caffeic acid and 0.02 g (12 mM) sodium hydride. The reactants were dissolved in the 1,4 dioxane solution and stirred at room temperature for 3 – 4 h. The resultant solution was filtered twice, evaporated and isolated by adding diethyl ether. The filtrate was collected (Na – caffeate). Bromo imidazole and sodium caffeate (1:1) were mixed together in a dual open neck round bottom flask and the flask was setup to pass the nitrogen gas through H₂SO₄. The mixer solution was stirred at 70 °C for 4 h. The viscous liquid with a tea color appeared and was characterized by NMR and FT-IR.

2.2.4(a) Characterization of FLVZ

FLVZ: ¹³C NMR (125.1 MHz, DMSO-*d*₆, δ, ppm); 30.55, 30.61, 30.71, 30.83, 48.04, 66.28, 119.16, 119.84, 122.38, 134.89. FT-IR (KBr, ν cm⁻¹); 3389 (OH stretch), 3008 (C-H_{arom}), 1832 (C=C_{aliph}), 1564 (C=C_{arom}), 1427, 1288 (CH₂ bending).

2.2.5 Characterization of sodium and silver rosmarinate: X-ray spectroscopy

Silver and sodium also were detected using the Tecnai T20 TEM engaged with the INCA energy dispersive x-ray spectrometer at 120 kV. Electron probes at 120kV voltage and 14° angle were used for this spectroscopy and counting time was 100 s.

2.3 Prediction of physicochemical properties

ACD ILAB ver 12.01 and PKCSM (Douglas et al., 2015) was used to determine the ADME and physicochemical properties of the new RA derivatives (NaR, AgR, FLVM, and FLVZ). The scores for <https://doi.org/10.25163/angiotherapy.21206512012110519>

oral and CNS activity are shown in supplementary Table S1 and they were set as the optimum value for the new analogues.

The logP (Octanol/Water), logD7.4 (Octanol/Water) for aqueous solubility and intrinsic aqueous solubility (logS), solubility at pH 7.4 (logS7.4), absorption, BBB penetration, P-gp transport, hERG inhibition, plasma protein binding and toxicity of the compounds were predicted before being tested experimentally. The computational program PKCSM version 1.0 was used to predict these properties. The prediction of efflux ratios for BBB was calculated using previously described algorithmic models (Khan et al., 2016).

2.4 Prediction of binding interaction with IL17A, VEGF and P-gp

The IL17A, VEGF and p-gp binding affinity and efficiency of the compounds were predicted using the LeadIT program windows version 2.1.9. The “flexible docking calculation” was used to predict the inhibitory potential of FLVM and FLVZ towards VEGF and IL17A. The binding activity and anti-angiogenic efficiency of the ligand with VEGF and IL17A were assessed using LeadIT ver 2.1.9 (<http://www.biosolveit.de/LeadIT/>). 3D crystal structures of VEGF and IL17A proteins were downloaded from the RCSB database (PDB code: 3QTK and 4HR9 respectively). The active sites of VEGF and IL17A were predicted using DoGSiteScorer (Volkamer et al., 2012). For VEGF, 19 pockets were detected and the most active pocket P0 was selected based on its high score of volume [Å³], surface [Å²], lipo surface [Å²], depth [Å], and simple score (2280.96, 2431.33, 1459.52, 27.59, and 0.64, respectively) relative to other pockets. Similarly, for IL17A, these scores were 1038.40, 1096.81, 713.19, 20.98, and 0.67, respectively. Chains B, C, E, and F of VEGF and A and B of IL17A were selected for the docking study. The ligand-protein interaction pose with lowest binding affinity was selected as the optimum effect of the compounds. The binding efficiency of the inhibitors was measured using hydrogen and desolvation (Hyde) energies. Molecular docking of the 3D crystal structure of P-gp (PDB code: 3G60) with the new derived compounds was performed using LeadIT. All molecular docking was performed three times. Molecular docking of P-glycoprotein (PDB code: 3G60) was performed with the new derived compounds.

2.5 Quantitative structure activity relationship (QSAR) and structure activity relationship (SAR)

QSAR of the compounds was determined using 37 training set compounds and 4 test set compounds using BuildQSAR ver 2.0. The QSAR was assessed by MLR analysis. To identify the mechanism by which these compounds (NaR, AgR, FLVM and FLVZ) act in cells, SAR was determined from their structure and chemical substituents. SAR was obtained from the molecular docking interactions between the substituents and the target molecule.

2.6 In vitro physicochemical properties

2.6.1 Thermal and chemical stability

The compounds were treated at 60 °C in an oven for 48 h within a glass chamber and incubated with LiOH (Khan et al., 2016a). The purity of the resultant compound was then determined by HPLC. To test chemical stability, the compound was mixed with aqueous HCL (pH 2.0) and Krebs-Heneseleit bicarbonate buffer (pH 7.4) at 37

°C for 2 h and again the purity of the resultant compound was detected by HPLC.

2.6.2 Stability in Human Serum

The compounds were mixed with the human serum (Sigma), (preheated at 37°C) with the resulting concentration of 0.5 mM (Khan et al., 2016a). The mixer solution (1000 µL) was then collected in a 2 ml tube. This serum solution was deprotonated using methanol (1 ml) and vortexed to mix properly. The solution was then centrifuged for 10 min at 10,000 rpm and filtered through a 0.45 µm PTFE filters (Biofil). The purity of the filtered compound was then determined by X-ray spectroscopy and RP-HPLC on a Agilent 1200 series coupled to a photodiode array detector (Agilent, CA, USA). The compound was quantified by the area of the peak, UV profile and retention time.

2.6.3 Ionization Constants (pKa) and Lipophilicity (logD 7.4)

The ionization constants of the compounds were determined by potentiometric titration with the GlpK_a apparatus (Sirius Analytical Instruments Ltd, Forest Row, East Sussex, UK). The ionization constants (pK_{as}) were measured by at least four separate titrations for each compound: different aqueous solutions (ionic strength adjusted to 0.15M with KCl) of the compounds (20 mL, about 1 mM) were initially acidified to pH 1.8 with 0.5 N HCl; the solutions were then titrated with standardized 0.5 N KOH to pH 12.2. All titrations were performed under an N₂ atmosphere and at controlled temperature (25.0 ± 0.1°C).

The partition coefficient for the neutral (un-ionized) form of the compounds (log P) and the distribution coefficient at physiological pH (log D^{7.4}) between *n*-octanol and water were obtained using the shake-flask technique at room temperature. In the shake-flask experiments HCl 0.1N and phosphate 50 mM buffers (pH 1.0 and 7.4 respectively) were used as aqueous phases. The ionic strength was adjusted to 0.15 M with KCl. The organic (*n*-octanol) and aqueous phases were mutually saturated by shaking for 4 h. The compounds were solubilized in the buffered aqueous phase at a concentration of about 0.1 mM and an appropriate amount of *n*-octanol was added. The two phases were shaken for about 20 min, by which time the partitioning equilibrium of solutes is reached, and then centrifuged (10000 rpm, 10 min). The concentration of the solutes was measured in the aqueous phase by UV spectrophotometer (UV-2501PC, Shimadzu). Each log P or log D value is an average of at least six measurement. All the experiments were performed avoiding exposure to light. The concentrations of FLVM and FLVZ were determined by our validated HPLC method.

2.7 Antioxidant properties

2.7.1 DPPH radical scavenging assay

The free radical quenching activity of the compounds and ascorbic acid (standard reference) were determined by the DPPH (Khan et al., 2013). The compounds were mixed with methanol (methanol:water as 1:1) and DPPH (100 µL, 200 µmol L⁻¹) and added in the mixer solution at room temperature for 30 min. The UV absorbance of the compounds were recorded at 517 nm and the EC₅₀ was calculated from the linear regression of the plotted percentage inhibition (I%) of below equation 2.3,

$$I\% = \left(1 - \frac{A_{\text{sample}}}{A_{\text{blank}}}\right) \times 100 \dots\dots\dots(2.3)$$

where, A_{blank} is the absorbance of the control reaction (containing all reagents except the test material).

2.7.2 FRAP assay

The antioxidant activity of the compounds was determined by the FRAP (Ferric reducing antioxidant power) (Benzie and Strain, 1996). FRAP working solution (300 mmol L⁻¹ acetate buffer, pH 3.6, 10 mmol L⁻¹ TPTZ in 40 mmol L⁻¹ HCl and 20 mmol L⁻¹ FeCl₃ in a ratio of 10:1:1) and compounds were mixed and kept for 8 min. The absorbance of the compounds was recorded at 600 nm using a Tecan microplate reader and the antioxidant activity was calculated as nmol Fe²⁺ equivalent amount of compound (µg) from the standard curve of ferrous sulfate (FeSO₄·7H₂O) (reference standard).

2.8 Cell based screening

2.8.1 Cell culture

MDCK, MDCK-MDR1 lines were collected from NIH, USA. Other lines of R28 were purchased from Kerastat, USA, and CCD 18co, HCT 116 and human endothelial cell line EA.hy926 were bought from the American Type Culture Collection (ATCC, Manassas, VA, USA) and human glioblastoma cell line U87 MG and DBTRG MG (multiple patient-derived cultures) were collected from the school of medicine, USM, Kelantan and cultured in Dulbecco's modified eagle medium (DMEM) (ATCC, USA) supplemented with 10% heat inactivated fetal bovine serum (HIFBS) (GIBCO), 100 units/mL penicillin-streptomycin (GIBCO), and 2 mM glutamine (GIBCO) in a humidified incubator with 5% CO₂ at 37 °C. HCT 116 cells were cultured in RPMI media with different contents of above supplemental (growth factors, serum etc). Rosmarinic acid (RA) and Avastin were purchased from Sigma (Germany). MTT (3-(4,5-Dimethylthiazol-2-yl)-2,5-diphenyltetrazolium bromide), trypsin, fibrinogen, aprotinin, phosphate buffered saline (PBS), and thrombin also were purchased from Sigma. Matrigel matrix (10 mg/mL) was obtained from BD Bioscience (USA). About 10 mg of the compounds (96% purity) was dissolved in sterile, cell-cultured tested DMSO (0.1%) (Sigma, USA) to prepare a 10 mg/mL stock solution, which was stored in a moisture controlled environment at RT. Other chemicals used were of analytical grade.

The human cell lines were cultured in DMEM medium (ATCC, USA) supplemented with 10% heat inactivated fetal bovine serum (HIFBS) (GIBCO, USA), 100 units/mL penicillin-streptomycin (GIBCO), and 2 mM glutamine (GIBCO) in a humidified incubator with 5% CO₂ at 37 °C. Rosmarinic acid (RA) and Avastin were purchased from Sigma (Germany). MTT, (3-(4,5-Dimethylthiazol-2-yl)-2,5-Diphenyltetrazolium Bromide), trypsin, fibrinogen, aprotinin, phosphate buffered saline (PBS), and thrombin were purchased from Sigma, Germany. Matrigel matrix (10 mg/ml) was obtained from BD Bioscience, USA. Roughly 10mg of 96% pure RA powder was dissolved in sterile, cell-cultured tested dimethyl sulfoxide (DMSO) (0.1%) (Sigma, USA) to prepare 10 mg/ml stock solutions which were stored in moisture controlled environment at room temperature. Other chemicals used were in analytical grade.

2.8.2 Cell viability assay

The human umbilical vein endothelial cell line EA.hy926 was used to screen the effects of compounds. MTT assay was used to perform the proliferation assays (Khan et al., 2016a). The human glioblastoma multiforme type IV cell line U87 MG was used to measure the anti-proliferative activity of the compounds. The effects of the compounds on IL17A production (1.56, 3.12, 6.25, 12.5, 25, 50 ng/ml) and on the proliferation of cancer and normal cell was also investigated. The study was conducted on 70% confluent cells seeded in the 96 wells plate. Cells were treated with six concentrations (6.25, 12.5, 25, 50, 100, and 200 µg/mL) of the compounds including Avastin (standard drug) in triplicates for 72 h at 37 °C and 5% CO₂. The MTT salt (20 µl of 5 mg/ml stock solution) was added after 72 h and again incubated for 4 h. The media of each well was discarded after 4 hours and DMSO (0.1%, 100 µl) was added in each well. The absorbance of the samples was recorded at 490 – 570 nm and the cell viability activity IC₅₀ was calculated by following equation 2.4,

$$\text{Inhibition} = 1 - \frac{\text{absorbance of treated}}{\text{absorbance of untreated}} \times 100 \dots\dots\dots(2.4)$$

$$\text{Proliferation} = \left(\frac{\text{absorbance of treated}}{\text{absorbance of untreated}} \times 100 \right) - 100 \dots\dots\dots(2.5)$$

The % inhibition was plotted against the concentration tested using Microsoft Excel, and the IC₅₀ was calculated using the regression analysis.

2.8.3 ROS activity

ROS reagent (fluorescent dye i.e. 2',7'-dichloro fluorescein diacetate (DCFH-DA) was used to determine the ROS expression in U87 MG cells. The expression and/or production level of the ROS was analysed on U87 MG cells according to previously described studies and details were described (Mohan et al., 2012). U87 MG cells were seeded in a 48 well plate for 2 days. At 80% confluence cells were treated with FLVM and FLVZ for 24 hour. Cells were washed with PBS and 100 µl ROS reagents (fluorescent dye i.e. 2',7'-dichloro fluorescein diacetate (DCFH-DA) was added in each well. Cells were incubated at 37°C for 30 min. Cell lysis buffer was added to the cells after the incubation period and centrifuged at 10,000 rpm for 10 min. Supernatant was collected and diluted with PBS and measured in a Tecan fluorescence microplate reader at 485 to 520 nm. Standard curves using a ROS standard were used to calculate the ROS concentrations in each experimental sample.

2.8.4 Ex vivo BBB permeability assay

BBB permeability of compounds was determined using MDCK-MDR1 cells (passage number 2, obtained from NIH, USA), which were seeded onto 0.33 cm² polycarbonate filters at a density of 60,000 cells/cm² and maintained in culture in 24-well plates according to a previously described protocol with slight modifications (Wang et al., 2005; Taub et al., 2005). Cells were grown for 3–4 d to become a confluent monolayer that expressed the P-gp after seeding, and their integrity was determined by measurement of the transepithelial electrical resistance (TEER, ohm square centimeter) with a volt-ohm meter (Millicell-ERS, Millipore Corporation, Billerica, MA, USA). The background TEER, that is to say the resistance of the filter alone was

subtracted, and only the cell monolayers with TEER > 1,000 Ωcm² were used (pre and post study). Cells were cultured with HBSS (Hank's balanced salt solution containing millimolar Hepes buffer, pH ~7.4) at 37 °C, which was incubated for 30 min with warmed HBSS. At first, HBSS was added to the receiver compartments and the compounds were independently added to the donor compartments at a concentration of 10 mg/mL DMSO (0.1%). Samples were collected from both the receiver and donor compartments after 90 min of incubation. Drug permeation across the monolayer was measured in both apical to basolateral (A–B) and basolateral to apical (B–A) directions. The apparent permeability, P_{app} (in cm s⁻¹) was calculated as following equation 1:

$$P_{app} = \frac{dQ}{dt} \times \frac{1}{(A \times C_0)} \dots\dots\dots(S1)$$

where $\frac{dQ}{dt}$ is the transport rate of the compound (moles per second), *A* is the area of the cell monolayer (centimeter square), and *C*₀ is the initial donor concentration (moles per liter).

2.9 Anti-angiogenic activity

2.9.1 Migration Assay

70% confluent EA.hy926 and U87 MG cells were used for the migration assay. A scratch wound was created in the middle of the well using a 0.1 ml pipette tip. After scratching the cell monolayer, detached cells were washed gently by PBS. The cells were treated with 4 concentrations (i.e. 2IC₅₀, IC₅₀, 1/2 IC₅₀ and 1/4 IC₅₀) of NaR, AgR, FLVM and FLVZ based on the IC₅₀ for 24 h. Avastin was used as standard reference. The percentage of inhibition of migration was calculated by measuring the gap (in Image J soft) of the scratch at 0h, 12h and 24 h on the photomicrograph. The percentage of inhibition was calculated relative to zero time using the equation below (3.1) and the results are displayed as average ± SD, (n = 6).

$$\% \text{inhibition (migration)} = 1 - \frac{\text{the width at zero time}}{\text{the width at the time}} \times 100 \dots\dots\dots(3.1)$$

2.9.2 Capillary-like tube formation assay

The 3D collagen (Matrigel, BD Bioscience, USA) with growth factors was used to form the tubes of the human umbilical vein endothelial cells EA.hy926. Matrigel (100 µl) was seeded in 48 well plates and incubated for 30 min at 37 °C. NaR, AgR, FLVM and FLVZ treated EA.hy926 cells (2IC₅₀, IC₅₀, 1/2 IC₅₀ and 1/4 IC₅₀ doses) were seeded into this matrigel. The network formation of the tubes was then monitored under a microscope after 16 h. Because of the effect of the new compounds, EA.hy926 cannot form the tubes and capillary network related to control. The branch points, number of tubes, covered area by cells were calculated from the web-based Image Analysis Win-Tube module of Wimasis software (Wimasis GmbH).

2.9.3 Rat aorta ring assay

Male Sprague Dawley Albino rats (180-220 mg, 6-8 weeks old) were collected from the USM animal house to perform rat aortic ring assays. Experiments were conducted according to animal ethics guideline approved by Animal Ethics Committee, Universiti Sains Malaysia (USM), Reference Number: USM/Animal Ethics Approval/2015/(658).

Aortic ring were used as angiogenic assay (Nicosia et al., 1990). Thoracic aorta were collected from male Sprague Dawley rates (12 – 14 weeks old). The cleaned aorta (removing fat tissue) was cut into small pieces and put in the membrane coated (M199 media supplemented with 3 mg/ml fibrinogen, 1 mg/ml aprotinin and 200 µl L-glutamin) 48 well plate. After seeding, the plate was incubated for 1 hour at 37 °C. Thrombin (10µl), (50 NIH U/ml in 1% bovine serum albumin in 0.15 M NaCl) was added into each well and reincubated at 37 °C for 1 hour to solidify. After forming the gel, the rings were treated with the NaR, AgR, FLVM FLVZ and Avastin at six concentrations (6.25, 12.5, 25, 50, 100 and 200 µg/ml) prepared in M199 media supplemented with 20% HIFBS, 0.1% 6-aminocaproic acid, 1% L-glutamine, 1% amphotericin B, and 0.6% gentamicin. The old media was discarded and rings were treated again at day 3. The length of the vessels outgrowth from the rings (primary tissue explants) was measured using Image-J software. The formation of vessel was affected by the new derivatives and percentage inhibition (IC₅₀) was calculated using a non-linear regression analysis as below equation:

$$\% \text{Inhibition (vessel)} = 1 - \frac{A_0}{A} \times 100$$

Where, A₀ = distance of blood vessel growth in treated rings in µm and A = distance of blood vessel growth in the control in µm.

2.9.4 CAM Assay

Chicken embryos at 5 – 7 days old were used in this assay following previously described methods with slight modification (Dohle et al., 2009). Eggs were wiped with sterile rough tissues to remove the feathers and dirt. The eggs were positioned vertically (towards long axis) and marked on the the wide upper side with a pencil since embryos are located in this area. The egg was then cracked by hitting this area (marked side). The shell was then delicately removed to make sure the egg (yolk and egg white) remains undamaged. The eggs were incubated at 37.5 °C and 60% humidity in the presence of sufficient O₂ supply. The new derivatives were applied on egg blood vessels at two concentrations (IC₅₀ and 1/2 IC₅₀). The eggs were monitored for 7 days and the inhibition of blood flow and affected vessels were observed by analysis of photomicrograph and the marked region.

2.10 IL17A and VEGF ELISA assay

The effect of NaR, AgR, FLVM and FLVZ against the expression of IL17A and VEGF (DuoSet ELISA Kit R&D Systems, USA) was assessed by sandwich ELISA assay in the U87 MG cells. 70% confluent U87 MG cells were treated for 48 h with NaR, AgR, FLVM and FLVZ. The cells were then lysed using 1 ml lysis buffer. The lysates were centrifuged and supernatant was collected and placed into the antibody-coated 96 well plate. The rest of the procedure was followed according to the instruction manual. The level of expression of the protein was calculated in comparison to a standard curve of IL17A and VEGF.

2.11 Apoptotic activity

2.11.1 Determination of nuclear condensation by Hoechst 33258 stain: 20,000 cells were seeded per well in 48 wells plate. After 48 hr , when 70-80% confluence was reached, U87 MG glioma cells were

treated with the compounds. Cells were fixed by adding 4%, paraformaldehyde in each well and incubated for 20 min. After incubation, the cells were washed with PBS and 100 µl of hoechst 33258 stain (1 µg/ml in PBS) was added. After 30 min of incubation, cells were observed under an inverted microscope to determine cell morphology. Cells with bright condensed nuclei and shrunken cytoplasm indicative of apoptosis were observed. These apoptotic cells were counted in four fields per well. The percentage of apoptotic cells were determined by following equation:

$$\% \text{Apoptotic index} = \frac{\text{number of apoptotic cells}}{\text{total number of live cells}} \times 100$$

2.11.3 Determination of mitochondrial potential: U87 MG cells were used to study the mitochondrial inhibitory potential of the compounds. Cells were treated as described in a hoechst staining assay. The only difference is that rhodamine 123 (5µg/ml PBS) was added prior to the hoechst. Definition and calculation of mitochondrial potential condition are similar to nuclear condensation as unhealthy mitochondria appear bright and shiny with irregular shapes.

2.12 Effect of RA derivatives on apoptotic targets of Caspase 3/ 7, 8, 9

The assay was carried out according to manufacturer’s instructions (Promega, USA). The cells were seeded in 96 well plates at 20 x 10⁴ cells/well in 200 µl medium and incubated for 24 hr to allow the attachment of cells. The treated cells were incubated for approximately 18 hr. Then, 100 µl of the caspase reagent containing cell lysis buffer and specific luminogenic substrate for caspase 3/7, 8 and 9 was added to each well. After incubating the plates for 30 min, the luminescence intensity was measured using microplate reader (Tecan, Switzerland). The effect of the compounds on caspase activity is represented by fold change upon treatment with NaR, AgR, FLVM and FLVZ. The fold changes in the caspase activity were measured by the following formula:

$$\text{Fold change} = \frac{L_s - L_b}{L_c - L_b}$$

where: L_s = Luminescence reading of wells treated with tested extract

L_b = Luminescence reading of blank

L_c = Luminescence reading of wells treated with vehicle

The results were stated as mean of fold changes in caspase activity in comparison to control ± SD (n=3).

2.13 In vivo detection of compounds in mice blood and brain

BALB/c male mice weighing 20-28 g were used for this experiment. Mice were treated with 50 mg/kg of NaR and AgR by oral gavaging of 500 µL of compound dissolved in 0.1% DMSO. After 2-4 hours, animals were euthanized and sacrificed to collect the blood and brain. Blood was collected by syringe from a heart punch into a test tube. The brain was removed immediately and rinsed with cold distilled water and homogenized at 4°C in an equal volume of water in respect to brain weight. After homogenization with a the Potter-Elvehjem homogenizer, an equal volume of acetonitrile containing 0.1% acetic acid was added to blood samples and brain tissue homogenates to precipitate proteins. The samples were sonicated, vortexed, and then centrifuged for 10min at 2150g. The clear

supernatant was filtered by 0.45 µm PTFE filters and analyzed by x-ray energy spectroscopy and HPLC.

2.14 Luciferase reporter gene assay (10 cancer pathways)

Luciferase gene reporter assay was conducted following Vikram et al. 2012. In brief, U87 MG cells were transfected using Trans Fact liposome transfection reagent (Promega, USA). Cells were incubated overnight and treated with the compounds Na⁺ and Ag⁺ salts. After 24 h, the luciferase reporter system was used to detect luciferase activity in a luminometer. Afterwards, firefly/renilla activity was determined in a luminometer. The fold change was calculated from the luminescence reading as following:

$$\text{Fold Change} = \frac{\frac{T_{\text{firefly}}}{T_{\text{renilla}}}}{\frac{C_{\text{firefly}}}{C_{\text{renilla}}}}$$

Where, T = treated and C = control

2.15 HPLC

The compounds were detected by HPLC. An HPLC analytical method was developed on Agilent 1200 series coupled to a photodiode array detector (Agilent, CA, USA). Chromatographic separation was achieved at room temperature (25°C) with a C4 reversed-phase column (Thermo Scientific™, USA 250×4.6 mm, 5-µM particle size) using a gradient solvent system that consisted of a mobile phase of acetonitrile and 0.05% formic acid, 50:50 (v/v), pH 5, running at an isocratic mode at flow rate 1.0 mL/min. The injected volume per sample was 100 µl and the total run time was 15 min. The absorbance was set at 200 – 450 nm and the UV measurements for quantification were performed at 220 nm. Quantification was carried out using HPLC retention time and UV spectrum of the analyte. The method was specific and sensitive with a lower limit of quantification of 1 ng/mL and the ChemStation LC3D software was used to ensure quantification of compounds. The variation of intraday and interday was minimal < 10%.

2.16 Statistical analysis

Microsoft excel 2013 and GraphPad prism V6.02 were used for statistical analysis. All data were evaluated with one-way ANOVA multiple comparisons test. A p value <0.05 was considered statistically significant. Data are reported as mean ± SEM.

3 Results and Discussion

3.1 Chemistry

The preparation of NaR, AgR, FLVM and FLVZ is depicted in scheme 1. The products were determined by the vibrational band of FT-IR and functional group peak of NMR. NaR was synthesized in a single step as depicted in the scheme 1 at room temperature under an inert environment. Use of inert environment is important since the presence of moisture may convert sodium hydride to sodium hydroxide which may ultimately hydrolyze the rosemarinic acid into two components instead of forming NaR. The isolated NaR was found to be very hygroscopic and was preserved in diethyl ether for further analysis and storage. FT-IR spectra of the compounds (NaR, AgR, FLVM and FLVZ) were collected using the KBr disc method. The KBr

discs were prepared quickly to avoid moisture accumulation and then thoroughly dried before collecting the spectra. In comparison, the FT-IR spectra showed significant changes in support of the formation of the required product. For example, the two vibrational bands for carbonyl groups in rosmarinic acid, labelled as 1 in Fig. S1, shifted to lower frequency as a broad single band which is in accordance to the formation of a sodium/potassium salt of organic acids (Jafari et al.,

2014; Syed et al., 2015). Furthermore, a few more changes may also be observed which indicated the formation of new product from the parent material. Further confirmation was done using NMR spectroscopy.

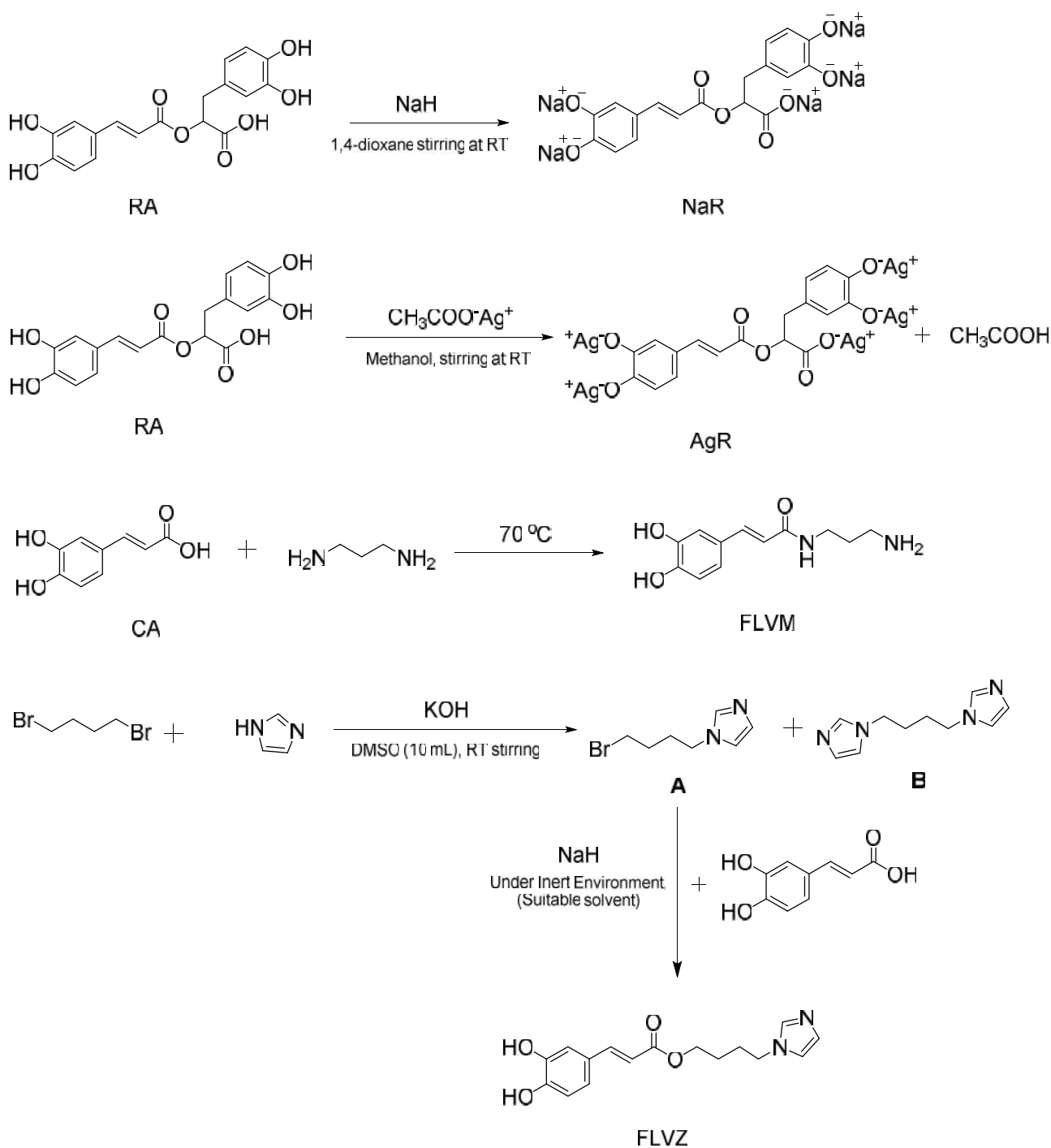
NMR (¹H and ¹³C) spectra of rosmarinic acid and NaR were collected using a 500 MHz NMR machine using DMSO-*d*₆ as solvent. ¹³C NMR spectra of both the compounds remained the same, whereas ¹H NMR showed distinct changes as can be seen in Fig. S2. The chemical shifts for carboxylic and phenolic protons which appeared in the range 8.5-10 δ ppm disappeared in sodium rosmarinate, indicating the replacement of phenolic protons by sodium ions.

In the synthesis of AgR, the most important step is the removal of unreacted silver acetate. Sometimes, filtration through celites becomes necessary more than 3 times to obtain a product in a purer form. The recrystallized product was dried at 60 °C for 24 hours. The dried product was preliminarily characterized by FT-IR and the spectral features of rosmarinic acid and AgR were compared (Fig. S2). Two vibrational bands (1727 and 1709 cm⁻¹) in rosmarinic acid can be seen to convert to a single vibrational band (1696 cm⁻¹) in AgR. This significant change provides a strong evidence for the formation of the required product. Furthermore, several noteworthy changes can be seen in Fig S3 which provide good indications of the formation of the required product. The synthesized compound was further characterized by NMR (¹H and ¹³C) spectroscopy. ¹H NMR of rosmarinic acid and AgR were compared. Both the spectra showed distinct changes in the region of 8-10 δ ppm. For example, the ¹H NMR spectrum of rosmarinic acid showed four chemical shifts in the region of 8-10 δ ppm, presumably due to the phenolic and carboxyl group protons. These chemical shifts were found absent in the ¹H NMR spectrum of AgR which indicated the replacement of protons by silver ions (Jafari et al., 2014; Syed et al., 2015). Sodium and silver salts were further confirmed by X-ray spectra (Fig. 9).

The synthesis process of FLVM and FLVZ is shown in scheme 1. In brief, 3-(3,4-dihydroxyphenyl) propanoic acid (caffeic acid) mixed with propane-1,3-diamine as 1:1 at 70 °C to produce the FLVM. A similar reaction of caffeic acid and 1-(4-bromobutyl)-1H-imidazole under nitrogen gas gave rise to FLVZ. The FTIR, NMR and HPLC spectra was shown in Fig. S4 (FLVM), Fig. S5 (FLVZ).

3.2 Physicochemical properties

Several computational QSAR models using NOVA, PKCSM and ACD I-LAB programs were utilized in the current study to predict the compound properties. The predicted properties of the new derivatives were deemed satisfactory for further screening and development. Despite the good results for the computational study, some deviation was found in vitro results. The solubility of the new E097-E122 | ANGIOTHERAPY | Published online May 11, 2019



Scheme 1. Synthesis of NaR and AgR at room temperature (RT). Synthesis of FLVM and FLVZ. 3-(3,4-dihydroxyphenyl) propanoic acid (A: caffeic acid) mixed with propane-1,3-diamine (B) in a ratio of 1:1 at 70 °C to produce FLVM. For FLVZ, in step-1, 1-(4-bromobutyl)-1H-imidazole was produced by the reaction between di-bromobutane and imidazole in the presence of KOH and DMSO at room temperature. A reaction between caffeic acid (E) and 1-(4-bromobutyl)-1H-imidazole (F) under nitrogen gas (step 2) produces FLVZ.

derivatives varied between salts of RA and bases of caffeic acid. The solubility of RA, NaR, AgR, FLVM, FLVZ was identical both in silico predictions and in vitro studies. The absorption (Water solubility (-2.62, -4.538, -0.992, -1.527log mol/L), Caco2 permeability (1.339, 0.414, -0.258, 0.978log 10⁻⁶ cm/s), intestinal absorption (0, 27.40, 62.82, 94.34% absorption), skin permeability (-2.74, -2.771, -3.471, -2.952log Kp), and positive p-glycoprotein substrate of the new derivatives were measured for NaR, AgR, FLVM and FLVZ

respectively. This data were found suitable for in vitro study (Table 1). The predicted BBB of NaR, AgR, FLVM and FLVZ was respectively -1.24, -1.585, -0.662, -0.996 in the PKCSM model, which showed the compounds as CNS active. The predicted efflux of the compounds was also determined by different algorithm and molecular docking binding data. The predicted efflux of the new derivatives was higher than RA. The predicted efflux ratio of NaR, AgR, FLVM and FLVZ were 4.44, 4.44, 4.48, 4.45, which kinds of significant results were determined in experimental efflux ratio of 22.35, 29.64, 32.49, 47.67, E097-E122 | ANGIOTHERAPY | Published online May 11, 2019

respectively (Fig. 7). Additionally, LD50, AMES toxicity, *T. Pyriformis* toxicity, minnow toxicity, maximum tolerated dose, chronic toxicity, hepatotoxicity, skin sensitization, and inhibitory potential of hERG I and II of the compounds were predicted and found to be non-toxic for all compounds. The predicted LD50 (as log of LD50) of NaR, AgR, FLVM and FLVZ is -0.05 mol/kg, 1.357 mol/kg, 1.881 mol/kg, 2.285 mol/kg, respectively (Table 1).

The stability of the compounds was determined from the fresh compound (with proper storage in non-aqueous media) and the mixer solution (1 ml final solution) with media, serum and chemicals by HPLC (supplementary HPLC chromatogram data). The compounds were measured from cell lysates of EA.hy926 and U87 MG cells and showed uniform distribution. The FITC labelled fluorescence photomicrographs (data not shown) confirmed the colocalization (with cellular fluids) of the salt and similar trafficking properties. These data suggest that endocytosed compounds remained intact in the cellular compartments, in serum (pH 7.4), in the presence of different chemicals and at high temperature.

The balance of the oxidative reactive species and antioxidant activity of the biological system could disfavor the preoxidant forces by producing oxidative stress. In particular, cancer and neurodegenerative diseases are associated with oxidative stress through LDL-oxidation (Aldred et al., 2010; Bennet et al., 2009; Hayashi et al., 2007). New compounds might display the antioxidant properties due to an increase in the lag time of TPTZ appearance and reduced the maximal rate of LDL oxidation catalyzed by metal complexes in the cell. We did not monitor the formation of hydroperoxides in the serum media. Further, all the newly synthesized derivatives (100 μ M) may have the ability to suppress conjugated diene formation during metal-mediated LDL oxidation. Serum auto-oxidation was initiated by the addition of 2.5 μ M Fe₂SO₄, and this was followed spectrophotometrically by detecting the formation of conjugated dienes at 234 nm. Typical results for this experiment are reported in the Table 2. The kinetics of LDL oxidation can be characterized using three parameters (Pinchuk and Lichtenberg, 2002) such as the determination of Δ lag time (Δt_{lag}) and the highest accumulation of oxidation products (OD_{max}). Δt_{lag} is the time period before onset of rapid lipid peroxidation (propagation phase) compared to control, and the propagation rate of the oxidation (R). New derivatives showed OD_{max} values similar to control. R and Δt_{lag} were determined from the corresponding curves for each compound shown in Table 2. We observed the most hydrophilic compounds with short alkyl group chains, cyclohexanes or benzene groups showed reduced R values compared to control. The lipophilic derivatives influenced the oxidation rate. Δt_{lag} also has negative effect on the lipophilicity and has positive effect on the hydrophilic compounds and determine the antioxidant activity. Δt_{lag} and logD_{7.4} showed the induction of iron lag time that may be due to LDL peroxidation. Furthermore, the lag time is influenced by the hydrophilicity and then reaches to plateau. In serum, LDL-iron complexes might formed by the binding of apolipoprotein. More and more complexes formed due to the availability of iron ions in the serum solution until a point at which all binding sites are saturated (Kuzuya et al., 1992). Due to formation of hydro-peroxides in the presence of LDL surfaces and iron, peroxidation is induced (Patel et al., 1997). RA and its derivatives

<https://doi.org/10.25163/angiotherapy.21206512012110519>

might sequester iron ions at physiological pH. The lipophilicity (logD_{7.4}) of the compounds compete for the distribution between LDL and aqueous phase. As a result, in this experimental condition, it is clear that the most hydrophilic compounds with higher amount of concentration (ligand or compounds) can be highly distributable in the aqueous phase free to iron ion complex which thus decreases the onset of lipidic peroxidation. We did not observe any considerable changes in ligand concentration in the aqueous phase due to the sequestering of LDL with the threshold value of logD_{7.4} at below -1 through further reduction of lipophilicity. Therefore, the chelation observe in the presence of iron ions validates the plateau. The lipophilicity and hydrophilicity of the compounds varied iron ion scavenging and thus the propagation rate of oxidation is also influenced.

The predicted properties were similar to the in vitro results for pKa, logP and logD_{7.4}, which were used to determine the absorption, distribution, metabolism, excretion and toxicity. The new compounds had predicted dissociation constants (pKa) of 2.79 (COOH), 9.45, 9.77 (m-OH), 12.33, 12.65 (p-OH) for RA. These prediction were almost identical to NaR and AgR which were pKa of 3.50 \pm 0.03, 8.17 \pm 0.03, 9.75 \pm 0.03, >12, >12 while the predicted pKas for FLVM and FLVZ were of 9.45 (m-OH), 12.31 (p-OH), 9.49 (m-OH), 9.76 (amine), 12.40 (p-OH) and 9.45 (m-OH), 12.31 (p-OH) respectively (Table 2). The sodium salt is highly soluble in the aqueous solution. The AgR was water soluble in warm condition but rapidly dissolved in methanol. Base compounds of FLVM and FLVZ were not aqueous soluble. FLVM and FLVZ were dissolved only in DMSO and lipid media. Other solvents such as methanol, ethanol and buffer (e.g. Acetic acid/sodium acetate buffers) were not suitable for dissolution of these compounds. The measurements of AgR, FLVM and FLVZ were carried out using methanol and DMSO as a co-solvent. Sensitive titration was conducted to determine the pKa value of the poorly water-soluble AgR, FLVM and FLVZ and the method also, suitable as cosolvent for dissolution. The predicted QSAR using ACD I-LAB analysis showed that the pKa of NaR and AgR had the strongest pKa(Acid) of 2.8 \pm 0.8 but no base pKa. The pKa values for FLVM was found as strongest pKa(Acid) of 9.4 \pm 0.4 and strongest pKa(Base) of 10.8 \pm 0.4 (data not presented in Table). The protonated, neutral and deprotonated status of the compounds were determined from the maximum and minimum absorbance. The salts existed as mono-charged cations which might form a mixture of non-zwitterion. Likewise, the bases were mono-charged anions and cations which may form a mixture of a zwitterion. The shake-flask lipophilicity studies of the compounds showed distribution coefficients (log D_{7.4}) that are reported in Table 2. Sodium and potassium salts are very highly hydrophilic and prevented the direct calculation of log D_{7.4} unlike AgR salt which showed moderate solubility in water. The molecular descriptors were calculated from the pKa and in pKcsm online calculator shown in Table 1. As expected, it increases because of the addition of lipophilic amine and imidazole substituents, while salts are most hydrophilic. These properties of pKa, logP and logD_{7.4} were used to determine the solubility, permeability, metabolism, protein binding and excretion of NaR, AgR, FLVM and FLVZ. The logD_{7.4} of the NaR, AgR, FLVM and FLVZ were -1.63 \pm 0.04, -1.64 \pm 0.05, -1.45 \pm 0.06, -0.33 \pm 0.06, respectively (Table 2) which describes moderate permeability and solubility. The pH status of the compounds could

E097-E122 | ANGIOTHERAPY | Published online May 11, 2019

determine the pharmacological and pharmacokinetics properties of the compounds and thus the results of pKa, logP and logD were shown to be effective for in vivo efficacy.

The binding interactions of the compounds were assessed using computational molecular docking study. These studies clearly show hydrogen bonding with the target molecules of IL17A and VEGF (Fig. 2). The hydrogen bonding and hydrophobic residue interactions were key determinants for BBB permeability. The above interactions showed the high hydrophobicity and hydrogen bonding is good criteria for BBB penetration. The IL17A and VEGF interactions with NaR, AgR were stronger than with rosmarinic acid and similarly stronger with FLVM and FLVZ compared to caffeic acid. The reason for this stronger interaction was the substitution of metal ions (the ions disassociate in solution and that have the anion or cation to interact with IL17A) and base functional groups (amine and imidazole). The activity was increased 2 to 20 folds in IL17A, and VEGF inhibition and antagonistic efficacy of the compounds (Fig. 2). The binding and efficiency significantly affected the biological efficacy for NaR (predicted binding of -40 KJ/mol, predicted efficiency of 0.37 Kcal/mol for IL17A, predicted binding of -28 KJ/mol, predicted efficiency of 0.26 Kcal/mol for VEGF, predicted binding of -30 KJ/mol, predicted efficiency of 0.28 Kcal/mol for P-gp), AgR (predicted binding of -27 KJ/mol, predicted efficiency of 0.25 Kcal/mol for IL17A; predicted binding of -21 KJ/mol, predicted efficiency of 0.19 Kcal/mol for VEGF; predicted binding of -30 KJ/mol, predicted efficiency of 0.27 Kcal/mol for P-gp), FLVM (predicted binding of -33 KJ/mol, predicted efficiency of 0.52 Kcal/mol for IL17A; predicted binding of -27 KJ/mol, predicted efficiency of 0.33 Kcal/mol for VEGF; predicted binding of -35 KJ/mol, predicted efficiency of 0.49 Kcal/mol for P-gp) and FLVZ (predicted binding of -30 KJ/mol, predicted efficiency of 0.36 Kcal/mol for IL17A; predicted binding of -32 KJ/mol, predicted efficiency of 0.38 Kcal/mol for VEGF; predicted binding of -35 KJ/mol, predicted efficiency of 0.42 Kcal/mol for P-gp) with IL17A, VEGF and P-gp (Table 3).

We determined the pharmacokinetic properties of the compounds in mice. The orally administered compound AgR (most active) (50 mg/kg once daily) showed a favorable PK with a C_{max} of 30 µg/mL, T_{1/2} of 1.53 h, and an MRT 2.21 (supplementary Table S8). The orally administered FLVM (most active) (50 mg/kg once daily) had a measured C_{max} of 14.65 µg/ml, T_{1/2} of 1.7 h (supplementary Table S8).

3.3 Effect of compounds on cell viability

To investigate the toxicity and protective effect of NaR, AgR, FLVM, FLVZ and IL17A, an MTT assay was conducted. Cancer cells (U87 MG and DBTRG MG) were treated with IL17A and then further treated with the new derivatives to understand the role of IL17A in cancer cells. Increased proliferation rates after IL17A treatment were observed (14.67%, 23.93%, 5.86%, 35.39% for U87 MG, MCF7, A549 and HCT 116 cells, respectively) compared to control at optimum dose of 25 to 12 ng/ml (Fig. 3-A – 3-H). We have observed the “U” shaped dose response curve for IL17A treated cells (Figure 3-A – 3-D). The IL17A (Fig. 3-E – 3-F) and VEGF (Fig. 3-G – 3-H) treated cells proliferated faster in absence of the secondary derivative compounds.

Furthermore, the new derivatives of NaR and AgR also showed cytoprotective activity in a serum deprivation assay. Moreover, NaR, AgR, FLVM and FLVZ did not produce any toxic effects at the concentration of <100 µg/ml (Fig. 4-A – 4-G). The toxic effects of the derivatives were only observed at high doses of >150 µg/ml (IC₅₀ of 154.44 µg/ml, 1285.14 µg/ml, 390.37 µg/ml, 208.21 µg/ml, 331.58 µg/ml, 532.83 µg/ml, 130.57 µg/ml for NaR, AgR, FLVM, FLVZ, RA, CA, and Avastin, respectively) (Fig. 4-H). Proliferation rates were unaffected in DBTRG at ~200µg/ml (Fig. 4-I). This concentration is not defined as cytotoxic according to the NIH cytotoxicity guideline (Geran et al., 1971) The slower proliferation rate of cells might come from the inhibition of IL17A in the culture medium or downregulation of cellular IL17A. All new derivatives showed dose independent growth effects in DBYTRG MG (Fig. 4-I) and dose dependent growth inhibition in U87 MG (Fig. 4-J) and EA.hy926 (Fig. 4-K) cells. The compounds were selective to glioma cells and vascular endothelial cells inhibition of proliferation (supplementary Table S2).

3.4 Anti-angiogenic activity of compounds

The effects of the inhibitor were analyzed to assess the anti-angiogenic activity. A series of cellular models were used to demonstrate the effect of NaR, AgR, FLVM and FLVZ as angiogenesis inhibitors. The effects of the compounds of endothelial and glioma cell migration was observed at every 6 h up to 24 h with complete disruption of cell migration (NaR: 59.83%, 44%; AgR: 60%, 63.80%; FLVM: 79.56%, 61%; FLVZ: 97.34%, 46.40% at 24 h for EA.hy926 and U87 MG, respectively) in treated cells compared to control (Fig. 5). FLVM and FLVZ had significant impacts on neovascularization as cells showed tubes showed notable disorganization and branching points showed improper lumen development (57% to 72% inhibition for NaR and 32% to 95% for AgR, FLVM: 81%, FLVZ: 82%) (Fig. 6-I, 6-II). In the co-culture assay, human endothelial cells (EA.hy926) were mixed with U87 MG cells conditioned media in a 3D collagen gel. The co-culture produced tubes of endothelial cells that were imaged and quantified to see the inhibitory effect of NaR, AgR, FLVM and FLVZ (Fig. 6-III). These co-cultured cells showed dramatic broken tube networks and pericytes covered the tubes after treatment with NaR, AgR, FLVM and FLVZ. Similarly, blood vessel formation was inhibited after the treatment of NaR, AgR, FLVM and FLVZ in the ex vivo rat aortic ring assay (IC₅₀ of 86.59 µg/ml, 49.69 µg/ml, 89.92 µg/ml, and 58.22 µg/ml for NaR, AgR, FLVM and FLVZ, respectively) (Fig. 6-IV). These effects are significantly different from untreated controls, rosmarinic acid and avastin. In chicken embryos, NaR, AgR, FLVM and FLVZ affected matured vessels and their branches (primary, secondary and tertiary vessels and dendritic branching pattern) after 24 h of treatment and the vessels were disorganized and unable to support consistent blood flow (Fig. 6-V). Moreover, both of the vessel formation and patterning at early and matured stage were disrupted in the presence of the compounds, suggesting a temporally-independent angiogenesis effect. Additionally, treatment of the embryos did not show any toxicity-induced cell lethality.

3.5 In vitro compound efflux and detection in mice serum and brain

To further demonstrate the BBB permeability of the new derivatives,

Table 1. Prediction of physicochemical properties of NaR, AgR, FLVM and FLVZ.

Predicted Properties		R. Acid	NaR	AgR	FLVM	FLVZ	C. Acid
Absorption	Water solubility(log mol/L)	-3.411	-2.62	-4.538	-0.992	-1.527	-1.144
	Caco2 permeability(log P _{app} in 10 ⁻⁶ cm/s)	-0.435	1.339	0.414	-0.258	0.978	0.274
	Intestinal absorption (human)(% Absorbed)	45.139	0	27.404	62.824	94.345	60.203
	Skin Permeability(log Kp)	-2.859	-2.74	-2.771	-3.471	-2.952	-2.976
	P-glycoprotein substrate	Yes	Yes	Yes	Yes	Yes	Yes
	P-glycoprotein I inhibitor	No	Yes	Yes	No	No	No
	P-glycoprotein II inhibitor	No	No	No	No	No	No
Distribution	VD _{ss} (human)(log L/kg)	-1.415	-0.65	-1.375	0.351	1.934	-0.848
	Fraction unbound (human)(Fu)	0.297	0.412	0.18	0.572	0.67	0.476
	BBB permeability(log BB)	-1.381	-1.24	-1.585	-0.662	-0.996	-0.751
	CNS permeability(log PS)	-3.507	-6.78	-3.659	-3.234	-2.996	-2.715
Excretion	Total Clearance(log ml/min/kg)	0.342	4.483	3.667	1.223	1.467	0.273
	Renal OCT2 substrate	No	No	No	No	No	No
Toxicity	AMES toxicity	No	No	No	Yes	Yes	No
	Max. tolerated dose (human)(log mg/kg/day)	0.924	0.811	0.636	1.343	0.748	1.426
	hERG I inhibitor	No	No	No	No	No	No
	hERG II inhibitor	No	No	No	No	Yes	No
	Oral Rat Acute Toxicity (LD50)(mol/kg)	1.727	-0.05	1.357	1.881	2.285	1.883
	Oral Rat Chronic Toxicity (LOAEL)(log mg/kg_bw/day)	2.296	3.768	2.354	1.778	1.754	3.09
	Hepatotoxicity	No	No	No	No	No	No
	Skin Sensitisation	No	No	No	No	No	No
	T.Pyriformis toxicity (log µg/L)	0.329	0.286	0.42	0.086	0.607	0.088
	Minnow toxicity(log mM)	1.453	1.22	-1.403	1.998	1.141	2.031

we conducted *in-vitro* efflux measurements to assess whether these compounds can enter the brain after oral administration (50mg/kg) in mice. *In-vitro* BBB permeability efficiency was determined using MDCK-MDR1 cells that we used as a CNS screening tool (Taub et al., 2005; Wang et al., 2005). The metal ions of NaR (22.35 efflux) and AgR (29.64 efflux) and lipophilic compounds of FLVM (32.496 efflux) and FLVZ (47.678 efflux) showed good BBB permeability with high efflux ratios (Fig. 7-A, 7-B). The efflux values could vary on the experimental level, the cell culture condition, and the expression level of P-gp. Avastin was used as the standard CNS positive drug. The compounds were considered to have good efflux ratios if their P_{app} (A-B) > 3 × 10⁻⁶ cm/s as of high potential to cross the BBB and P_{app} (A-B) < 1 × 10⁻⁶ cm/s as of low potential. Moreover, efflux ratio varied due to the unbound P-gp fraction. To determine the BBB permeability of the compounds in mice, blood and brain samples were collected after 2-3 hours and proteins were isolated using methanol and acetonitrile. Samples were injected in the HPLC and content was determined by the validated HPLC method. The concentration of (1.5±0.18 µg/g tissue), AgR (3.75±0.56 µg/g tissue), FLVM (2.68±0.71 µg/g tissue) and FLVZ (3.05±0.33 µg/g tissue) were found at 2 hours in the brain.

In the blood, all derivatives were detected at 2.5±0.37 µg/mL after 2 hr and 1.01±0.07 µg/ml after 3 hr on average (data not presented graphically).

From this data, it can be concluded that the salt and base rosmarinates increased in concentration in the brain while decreasing in concentration in the blood.

3.6 Inhibition of VEGF, IL17A, HIF1α, pRb-E2F, MAPK/ERK in U87 MG glioma

We assessed the effect of compounds on IL17A and VEGF expression. The ELISA assay showed a > 2-fold downregulation of VEGF and IL17A (Fig. 7-C). This effect on bio-markers reveals the anti-angiogenic activity of compounds. To determine the molecular pathways of the compounds, we conducted a reporter gene array on 10 cancer pathways. NaR showed -1.14-fold downregulation of MAPK/ERK and AgR showed 4.79-fold upregulation of pRb-E2F in reporter gene array (Fig. 7-D). FLVM showed -1.73-fold downregulation of Myc/Max gene. Interestingly, NaR, AgR and FLVM showed downregulation of HIF1α gene (Fig. 7-D). In addition, caspase levels are upregulated after treatment with NaR, AgR, FLVM

Table 2. Physicochemical properties [pKa, log P and log D (octanol/water system)], and antioxidant properties (radical scavenging, and FRAP activities) of NaR, AgR, FLVM, FLVZ, RA, and CA.

Compound	DPPH EC ₅₀ (µg/mL)	FRAP without Serum (nmol Fe ²⁺ eq./mg)	FRAP with Serum (nmol Fe ²⁺ eq./mg)	Δt _{lag} (min) ±SEM	R (nmol min ⁻¹ mg ⁻¹ LDL prot) ±SEM	pK _a		log P _{oct} (neutral form)		log D _{oct} ^{7,4}
						predicted ^{a)}	experimental ^{b)}	predicted ^{d)}	experimental ^{d)}	experimental ^{d)}
NaR	28.76±0.12	37.01±0.38	294.83±1.61	82±2	5.8±1	f)	f)	-	1.71 ±0.04	-1.63 ±0.04
AgR	13.91±0.10	46.54±0.66	80.76±2.92	48±3	12±2	f)	f)	-	1.73 ±0.06	-1.64 ±0.05
FLVM	12.90±0.07	89.41±0.15	400.83±11.718	78±3	9±2	9.49 (<i>m</i> -OH) 9.76 (amine) 12.40 (<i>p</i> -OH)	9.12 ±0.05 10.3 ±0.06 >12 ^{c)}	0.11	-	-1.45 ±0.06
FLVZ	9.44.39±0.42	31.39±0.42	497.47 ± 1.717	65±3	7±3	7.0 (imidazol) 9.45 (<i>m</i> -OH) 12.31 (<i>p</i> -OH)	ui6.05 ±0.03 9.66 ±0.03 >12 ^{c)}	1.59	-	-0.33 ±0.06
Rosmarinic acid (RA)	9.01±0.21	40.12±0.52	354.19±9.39	83±2	6±3	2.79 (COOH) 9.45, 9.77 (<i>m</i> -OH) 12.33, 12.65 (<i>p</i> -OH)	3.50 ±0.03 8.17 ±0.03, 9.75 ±0.03 >12, >12 ^{c)}	1.70	1.75 ±0.05	-1.58 ±0.08
Caffeic Acid (CA)	3.31±0.96	75.13±2.22	388.26±14.34	55±5	6±1.8	4.04 (COOH) 9.97 (<i>m</i> -OH) 12.79 (<i>p</i> -OH)	4.46 ±0.02 9.19 ±0.02 >12 ^{c)}	1.42	1.46 ±0.03	-1.27 ±0.03
Ascorbic acid	7.30 ±0.01	ND ^{g)}	ND ^{g)}			ND ^{g)}	ND ^{g)}	ND ^{g)}	ND ^{g)}	ND ^{g)}

- a) Calculated with ACD/Labs pKa DB vers. 7.00 program (Advanced Chemistry Development, Inc.)
- b) Measured by Sirius GIpKa by aqueous titration
- c) Calculated by ACD/Labs log P DB vers. 8.00 program (Advanced Chemistry Development, Inc.)
- d) Measured by shake flask technique (aqueous phase buffered at pH 1.0 for log P and pH 7.4 for log D)
- e) pK_a greater than 12 cannot be measured accurately
- f) the data obtained are identical to those of RA
- g) ND (not detected)

Table 3. Computational study of NaR, AgR, FLVM, and FLVZ on IL17A, VEGF and p-gp binding and efficiency. P-gp binding was used to predict the efflux ratio.

Compounds	IL17A		VEGF		p-gp	
	Binding ^{a)} (Kj/mol)	Efficiency ^{b)} (Kcal/mol)	Binding ^{a)} (Kj/mol)	Efficiency ^{b)} (Kcal/mol)	Binding ^{a)} (Kj/mol)	Efficiency ^{b)} (Kcal/mol)
Rosmarinic A.	-37	0.29	-22	0.20	-29	0.26
NaR	-40	0.37	-28	0.26	-30	0.28
AgR	-27	0.25	-21	0.19	-30	0.27
FLVM	-33	0.52	-27	0.33	-35	0.49
FLVZ	-30	0.36	-32	0.38	-35	0.42

- a) Predicted
- b) Predicted

and FLVZ in apoptotic cells (Supplementary Table S3). The effect of caspase provides the apoptotic effect of the compounds on cancer cells. Cancer cells die due to increased levels of ROS by NaR and AgR. On the other hand, FLVM decreased ROS level and caused apoptosis. The apoptotic index of the cells was determined using Hoechst and rhodamine staining. Fragmented nucleus and mitochondrial membranes were found after treatment with NaR, AgR, FLVM and

FLVZ (Fig. 7-F, 7-G).

3.7 QSAR

A QSAR model was constructed to compare the biological activity of the compounds. The dataset of the QSAR is shown in supplementary Table S6. The QSAR model revealed an R² value of

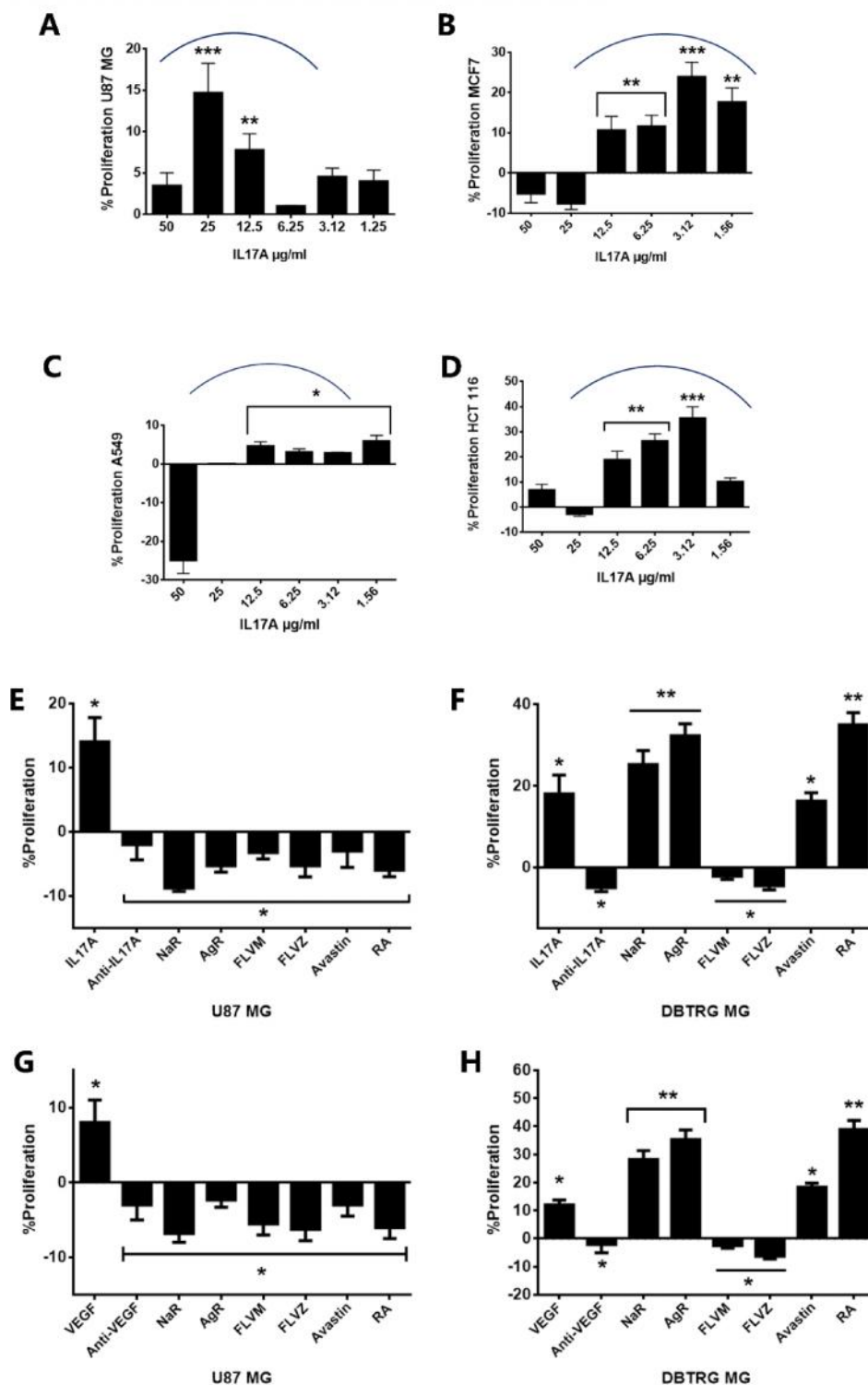


Fig. 3. Effect of IL17A on the proliferation of U87 MG (A) and other cancer cells MCF7 (B), A549 (C) and HCT 116 (D). Comparative anti-proliferative effect of the IL17A, VEGF, anti-IL17A mAB, anti-VEGF mAB and NaR, AgR, FLVM, FLVZ in two glioblastoma cell lines U87 MG and DBTRG MG.

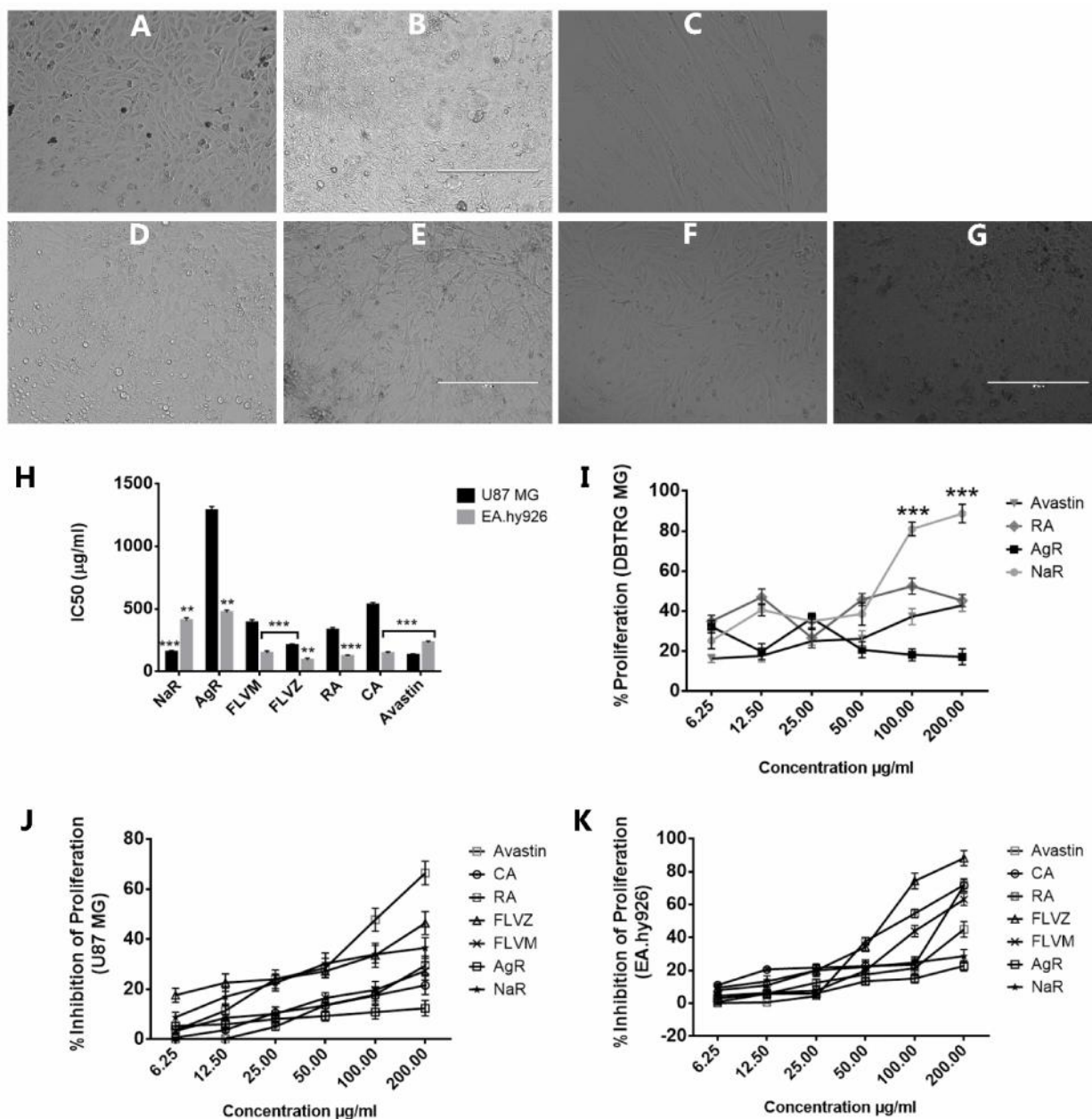


Fig. 4. Photomicrographs of cell viability after AgR treatment in various normal and cancer cell lines such as EA.hy926 (A), MDCK (B), CCD 18 co (C), R28 (D), U87 MG (E), DBTRG MG (F), HCT 116 (G). The other derivatives of NaR, FLVM and FLVZ show almost identical photomicrographs. Inhibitory concentration of NaR, AgR, FLVM and FLVZ in U87 MG and EA.hy926 cell lines (H). The effect of these derivatives on proliferation of DBTRG MG (I). The percent inhibition of growth by the derivatives in U87 MG (J) and EA.hy926 (K) cell lines. The compounds showed cytotoxicity at very high dose (more than >150 µg/ml). This concentration is defined as chemo compound.

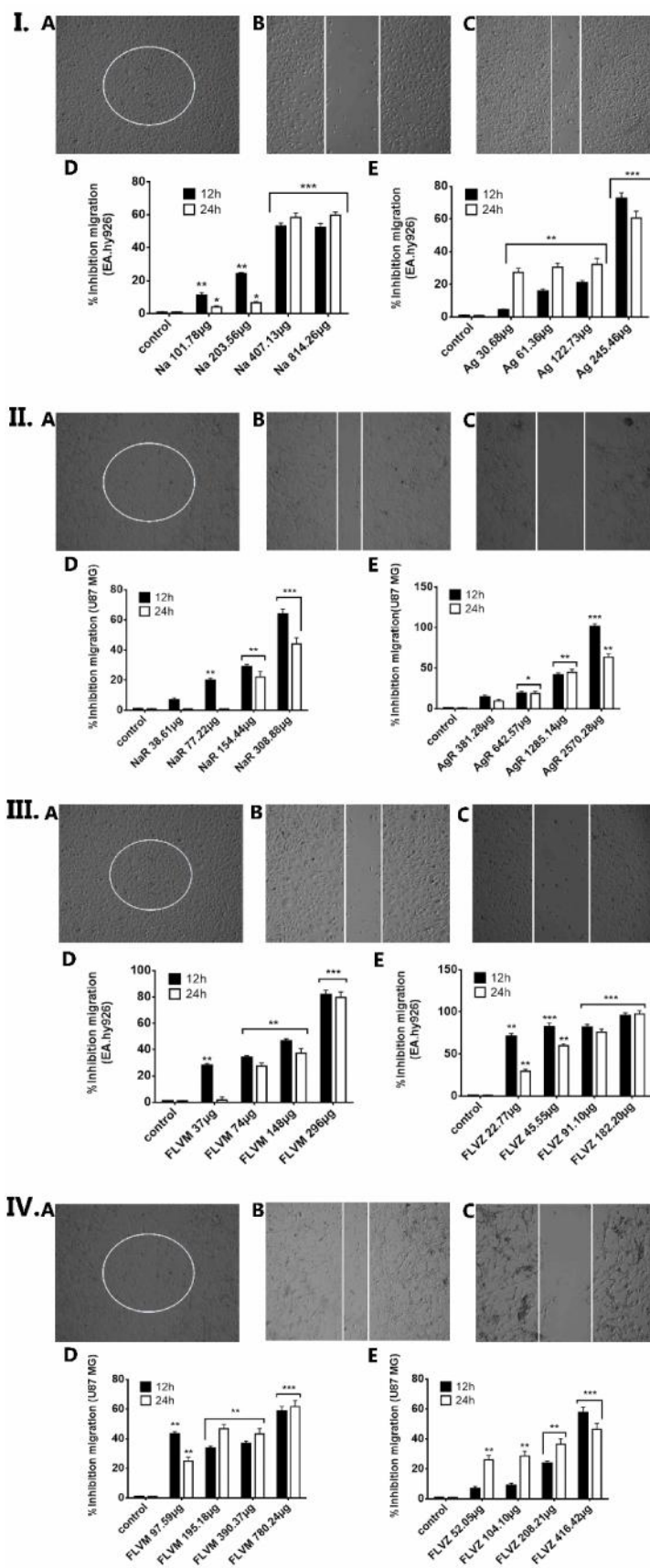


Fig. 5. Anti-migratory effect of NaR, AgR, FLVM and FLVZ on cell migration of EA.hy926 and U87 MG cell lines. The photomicrograph reveal the effect of compounds after 24 h. (A) control and (B), (C) after treatment.

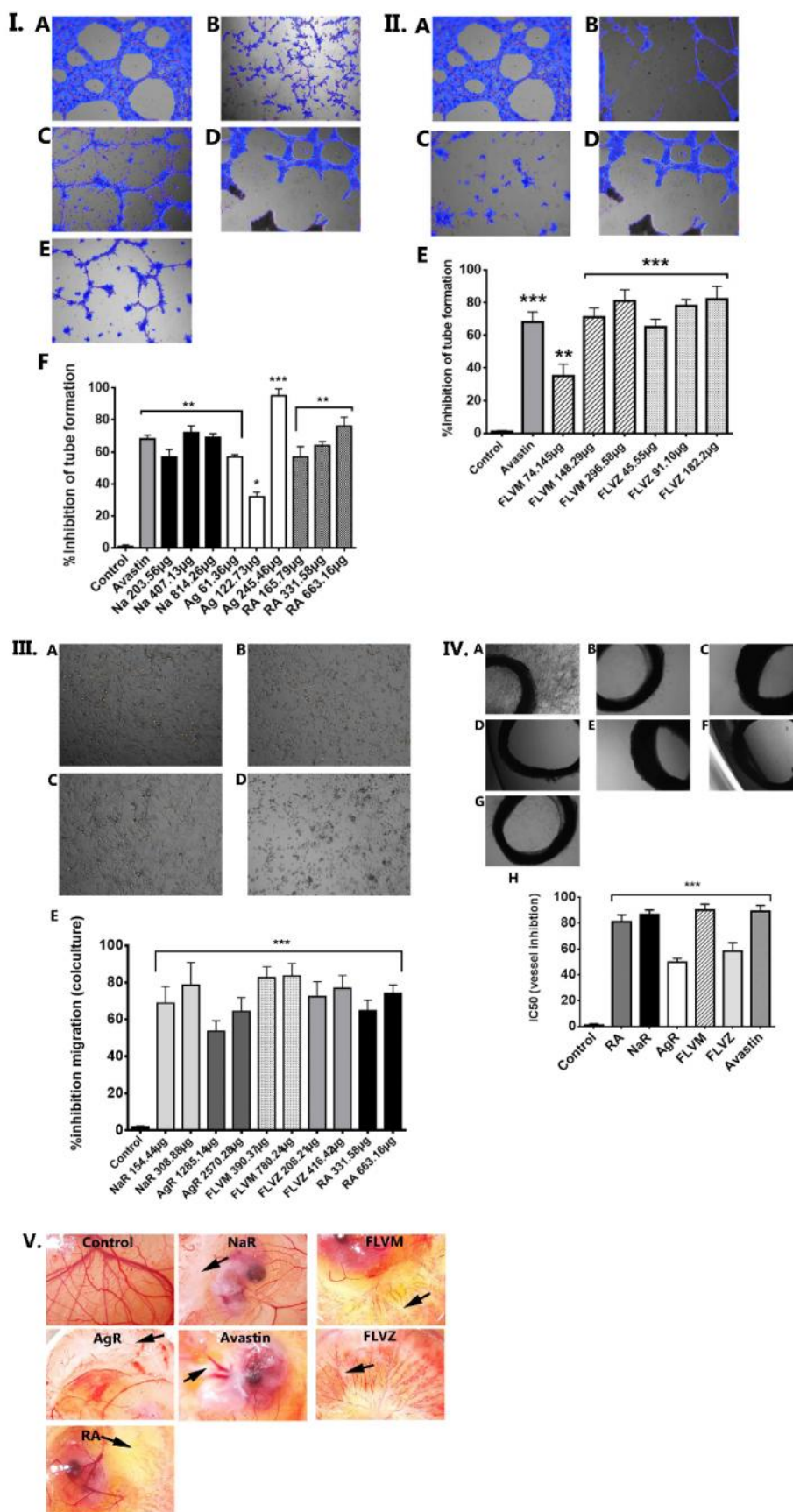


Fig. 6. Inhibitory potential of new derivatives on capillary-like tube networks of EA.hy926. I-A: control; I-B: NaR; I-C: AgR; I-D: Avastin; I-E: RA, I-F: graph; II-A: control; II-B: FLVM; II-C: FLVZ; II-D: Avastin; II-E: graph. Anti-migratory effect of the new derivatives on U87 MG induced migration of EA.hy926 cells. IIIA: NaR, IIIB: AgR; IIIC: FLVM; IIID: FLVZ. Representative photomicrograph of aortic rings for control (IVA), RA (IVB), NaR (IVC), AgR (IVD), FLVM (IVE) and FLVZ (IVF) and Avastin (IVG) and their inhibitory concentration (IVH) against aortic explants. Inhibitory potential of NaR, AgR, FLVM and FLVZ in angiogenesis of CAM (V). Values represented the average of three separate experiments (n = 6). Bars represent the value as mean ± SEM. Asterisk represents the p value as *P < 0.05, **P < 0.01, ***P < 0.0001 as significant value.

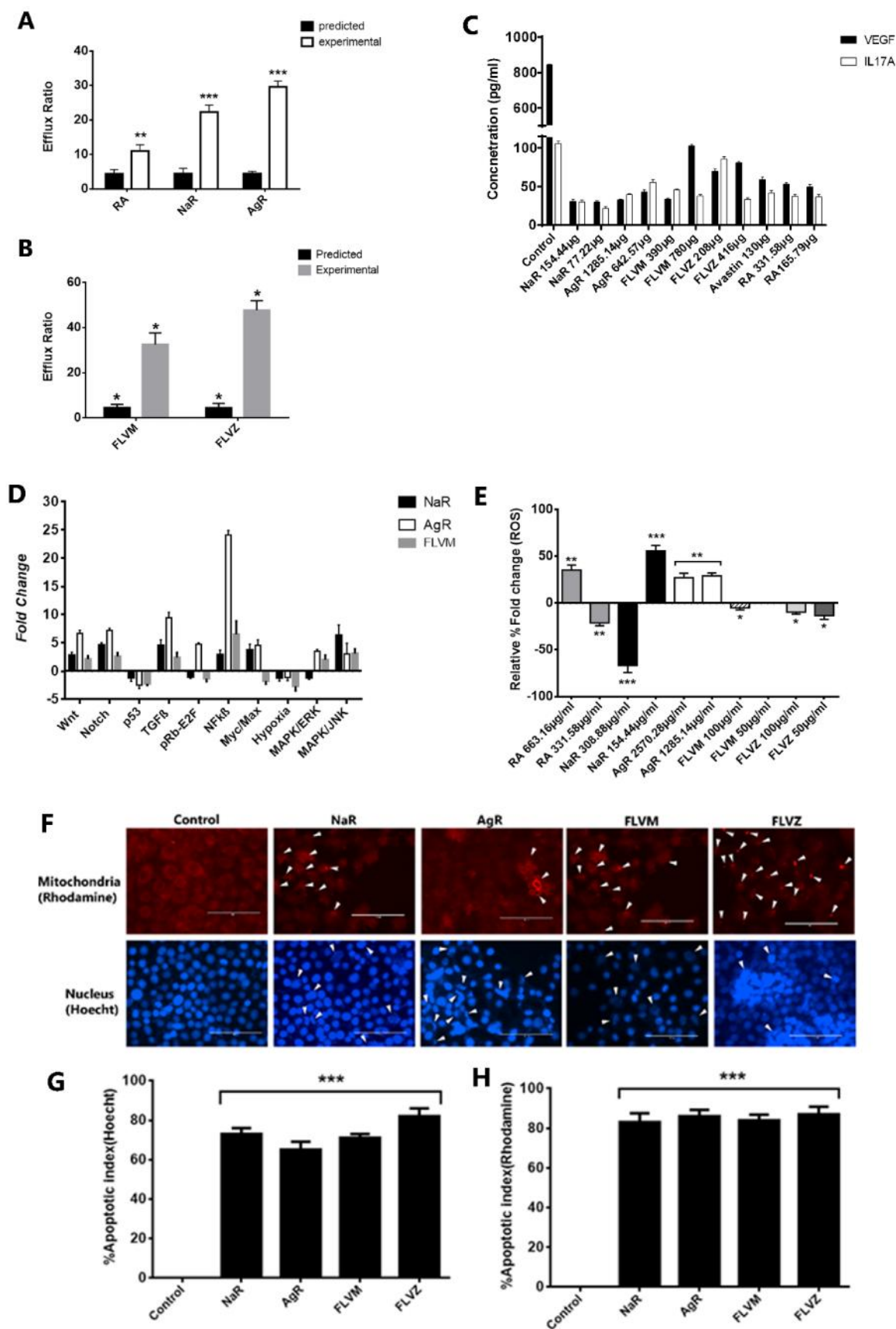


Fig. 7. Blood-brain barrier permeability of NaR, AgR, FLVM and FLVZ (A), (B). *In-vitro* blood-brain barrier permeability experiment was developed using the MDCK-MDR1 cells. NaR, AgR, FLVM and FLVZ significantly affected the VEGF and IL17A expression in U87 MG cells *in-vitro* (C). Luciferase gene reporter array (A, B) and western immunoblot (C, D) of NaR, AgR, FLVM and FLVZ. (D). Effect of the RA derivatives on intracellular ROS of U87 MG cells (E). Apoptotic morphology of U87 MG cells after treatment (F).

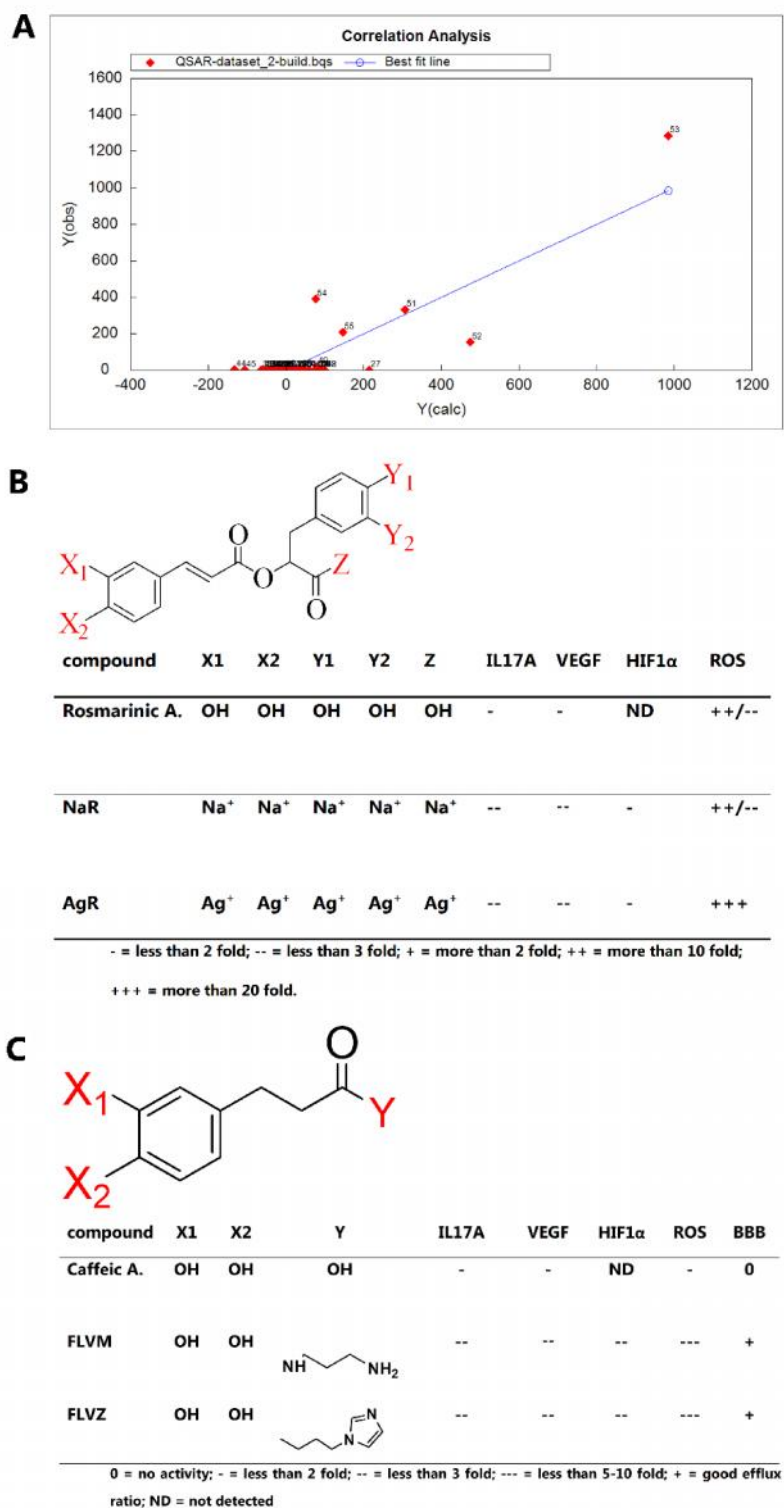


Fig. 8. (A) QSAR model of the compounds. (B) SAR of NaR and AgR. (C) SAR of FLVM and FLVZ. Structure–activity relationships is determined through the structural substituents by comparing the IL17A, VEGF, HIF1 α and ROS activity.

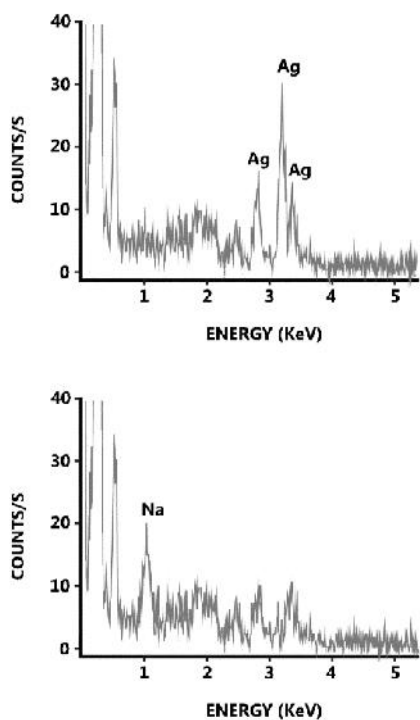


Fig. 9. Characterization of NaR and AgR by X-ray spectra which was used for detection of Ag⁺ and Na⁺ in brain tissues, plasma and cell lysates. Spectra were determined by the energy dispersive X-ray emission spectroscopy.

0.7429, and Q² value of 0.0323, as the internal cross-validation of the model. The QSAR equation is mentioned below.

3.7.1 QSAR equation:

$IC_{50} = - 32.7744 (\pm 33.8734) MW - 32.7684 (\pm 13.3042) pIC_{50} + 1.2815 (\pm 0.3474) Mol. Weight - 9.7731 (\pm 28.1871) Clean Energy - 27.1259 (\pm 29.6851) LogP + 1.0117 (\pm 1.3045) PSA - 4.6798 (\pm 193.3810).$

$(n = 55; R = 0.862; s = 100.163; F = 23.115; p < 0.0001; Q_2 = 0.032; SPress = 194.320; SDEP = 183.207).$

3.8 SAR

SAR was measured as a comparative analysis of the effects of each compound depending on their structure. (Fig. 8). The activity was increased after substitution of metal ions sodium with silver and amines with imidazole. The inhibitory potential of IL17A, VEGF, HIF1 α and ROS were > 2-fold after treatment but NaR and AgR showed increased ROS levels.

3.9 Biological efficacy

3.9.1 Selective efficacy of the salt and base rosmarinates in glioblastoma

Despite many compounds and drugs being investigated for the treatment of cancer, cancer prevalence is growing continuously and most treatments only inhibit its progression for a certain while. Suboptimal therapies can prolong patient survival but a true cure is still far away. The anti-cancer efficacy of drugs and natural compounds currently being used are limited and furthermore, they can have toxic effects on healthy tissue. Moreover, the anti-angiogenic compounds provide very slow activity after administration. Some specific cytokines are overexpressed by every cancer to survive and become drug resistant. During resistant, cancer cells also change their cytokine-dependent survival pathways. In this regard, we found that

<https://doi.org/10.25163/angiotherapy.21206512012110519>

metal and some other chemical fragments could be useful to enhance the anti-cancer activity of drugs via targeting the overexpressed pathogenic IL17A cytokine and its downstream angiogenic pathways. In the current study, we harness such anticancer efficacy by designing 4 derivatives of rosmarinic acid and its ester caffeic acid.

GBM is highly angiogenic through IL17A signaling pathway. The suppressing of this molecular signals could be a direct mechanism to inhibit its downstream angiogenesis in GBM. IL17A is found to be highly expressed in medulloblastoma tissues derived from infiltrating T cells (Zhou et al., 2010), and increased IL17A mRNA expression is reported in human gliomas (Wainwright et al., 2010). Furthermore, the dynamics of CD4⁺ T cells in the presence of other cytokines such as vascular endothelial growth factor (VEGF), transforming growth factor (TGF)- β , TNF- α , IL1, IL2, and interferon (IFN)- γ in the tumor microenvironment are widely variable (Paladugu et al., 2013). The IL17A, VEGF and HIF 1 α proteins are key component of multiprotein chaperon complex which includes p23, Cdc37, JAK, STAT, kinase proteins and others to regulate the folding, maturation, stabilization and renaturation of the client proteins (Neckers and Ivy, 2003; Pratt and Toft, 2003). To inhibit the downstream angiogenesis activity of the client proteins in tumorigenesis and disruption of IL17A controlled pathways could lead a great impact on cell growth and susceptibility to apoptosis. Computational prediction for physicochemical properties (solubility, lipophilicity, toxicity and BBB permeability) and significant molecular docking binding with IL17A and VEGF showed the first measure of salt and base rosmarinates efficacy. The reason may be due to electrostatic charge, and Van Dar Waal's force and hydrophobic characteristics of the molecules. RA derivatives showed their binding interaction through ionic bonds, phenolic groups, amine and imidazole groups. The RA derivatives showed the inhibition of VEGF

E097-E122 | ANGIOTHERAPY | Published online May 11, 2019

and IL17A which might be due to antagonistic efficacy of the compounds in biological microenvironment. Further, the disruption of upstream protein activity such as Hsp90, p23, Cdc37 etc towards the angiogenic signals of VEGF and IL17A might be crucial also to affect their expression in tumor microenvironment (Khan et al., 2016b). Interestingly, the RA derivatives showed their effect in HIF1 α pathway and inhibit the GBM proliferation. This result related to the ROS effect of compounds that was significantly upregulated after sodium and silver salts treatment but significantly downregulated after FLVM and FLVZ treatment. This findings related to the prevention of auto-oxidation of tumor tissues through inhibiting immune cytokines. RA derivatives showed inhibition of endothelial cell proliferation, migration, invasion, tube formation, and CAM and rat aortic angiogenesis in in-vitro study. The disruption of angiogenesis might block the oxygen and nutrient supply to GBM cells which caused the apoptosis of GBM cells. The apoptotic activity of RA derivatives was found in caspase 3/7, 8 & 9 activity. The upregulation of caspase in the treated cells was the reason of apoptosis, too. This effect was further, observed in in-vitro Hoechst 33258 and Rhodamine 123 staining assay which showed nuclear fragmentation, chromatin condensation, and mitochondrial membrane damage in GBM cells. The apoptotic activity was selective as > 2 fold for endothelial and GBM cells. In addition, the safety of the derivatives also, was recommended as safe CNS drug since the obtained overall IC₅₀ was > 100 μ g/ml while the effective antiangiogenic dose was < 50 μ g/ml. The salts rosmarinates showed the IC₅₀ at > 200 μ g/ml. In particular, the IC₅₀ of silver salt was >1200 μ g/ml. This data showed the non-toxic effect of these salts. The base derivatives also, showed similar non-toxic effects. The compounds anti-GBM efficacy was highly potential in compared to Avastin (bevacizumab). The IL17A mediated angiogenesis targeted results indicated that apoptosis was due to blocking of the nutrient supply to the mitochondria and nucleus by RA derivatives. As a result, a significant decrease in Rhodamine fluorescence intensity was observed in the activation of apoptosis (Polla et al. 1996). In addition, the rationally designed RA derivatives acted on the inflammatory pathways and provided anti-GBM efficacy in brain microenvironment due to their optimum blood-brain barrier permeability. The reason behind this is due to metal ions, amine and imidazole that make able the derivatives to pass BBB (Khan et al., 2016). We conducted in vitro BBB permeability tests using MDCK-MDR1 cell model, as CNS screening tools (Wang et al. 2005; Taub et al. 2005) and Avastin (bevacizumab) was used as the standard CNS positive drug. Celastrol was used as another reference compound as IL17A targeted molecule in our previously published study (Khan et al., 2016b) which revealed that RA derivatives provided significant efficacy in compared to Avastin, Celastrol and control. Furthermore, the in-vivo efficacy of these compounds were also, found highly potential for the treatment of GBM (submitted manuscript, Khan et al, 2017). However, this current study revealed the design, synthesis and mechanism of salts and base rosmarinates as IL17A inhibitor against GBM and their use thereof.

3.9.2 Effect of RA derivatives in GBM micro-environment

RA derivatives showed their antiangiogenic efficacy and apoptotic activity in cellular *in vitro* assays which was further analyzed in angiogenic and apoptotic target assays. ELISA assays were used to <https://doi.org/10.25163/angiotherapy.21206512012110519>

determine the expression of VEGF and IL17A proteins in U87 MG cells treated with RA derivatives, and the results indicated the inhibition of the IL17A and VEGF expression. RA derivatives may suppress the activity of IL17 expression through chelation, protonation or a methylation mechanism and may hinder upstream protein activity such as Hsp90 and p23 (Khan et al. 2016b). Additionally, RA derivatives can minimize glioblastoma vascularization by inhibiting IL17A downstream proteins VEGF, EGF, and IL6 to block the formation of a vascular bed. The likely reason of this effect might be the blocking of IL17AR via inactivation of Hsp90 or p53 which then inhibits signaling through JAK and STAT-3 phosphorylation (Tuettenberg et al. 2006). The ROS assay showed significant increased levels of ROS in salt rosmarinate-treated GBM cells and significantly decreased levels of ROS in base rosmarinate-treated GBM cells compared to control. Both the accumulation and inhibition of extreme levels of ROS can cause apoptosis of GBM cells due to the silencing of redox protein, Hsp90, G2/M cell cycle arrest which then results in DNA and mitochondrial damage and tumor angiogenesis suppression (Zhang et al. 2011, Pathi et al., 2011). In the reporter gene assay, we found inhibition of HIF1 α , MAPK/ERK, pRb-E2F, and Myc/Max gene after treatment of GBM cells by RA derivatives. The modulation of these key target was the reason for the RA derivative anti-GBM activity. Increasing ROS levels can activate MAPK/ERK and modulate p27 and pRb-E2F pathways in a complex cascade and this presumably hinders cell growth (Torres and Forman 2003; Matsuzawa and Ichijo 2008; Okoh et al., 2015; Kay 2008; Nevins 2001). RA derivatives inhibit IL17A and HIF1 α *in vitro* in GBM cells. These two cancer bio-markers are important convergent points upstream of VEGF signaling in tumor angiogenesis. Tumor infiltrating immune cells release a large amount of IL17A into the tumor microenvironment to upregulate VEGF, IL10, ANG-1/2, IL2, IL8 (Angelo and Kurzrock 2007). Due to the inhibition of HIF1 α , GBM cell cannot induce angiogenesis and reduce their apoptosis. The RA derivatives activate MAPK/ERK and pRb-E2F through ROS activation which contributed to the inhibition of HIF-1 α synthesis, HIF-1 α stability, and HIF-1 α transactivation (Georgina and Wei, 2015). We found that inhibition of HIF1 α , VEGF, IL17A and activating of ROS produced a potent anti-angiogenic effect in tumor-mediated neovascularization, tip and pericyte formation and thereby apoptotic activity. The FDA has recently approved ROS generating monoclonal antibody based drugs for brain tumors. A similar kind of pro-oxidative, apoptotic and anti-angiogenic mechanism is also observed in RA derivatives (Oztekin et al., 2012).

4. Conclusion

In conclusion, this study demonstrated the development of rosmarinic acid and computer aided design, chemical synthesis and anti-GBM properties of synthetic RA derivatives which showed modulation of IL17A downstream angiogenesis could be targeted by RA and its derivatives which could be suggested to use in glioblastoma patient. The RA and its derivatives can be classified as safe anti-angiogenic chemotherapy unlike traditional chemo drugs and we report it for the first time as an anti-GBM candidate drug with a mechanism involving apoptosis and anti-angiogenesis.

Author Contribution

M. S. S. Khan designed the research idea, planned, conducted experiments on cytotoxicity, adipogenesis and angiogenesis screening, synthesizing the RA derivatives (NaR, AgR, FLVM & FLVZ), plasma metabolites screening and analysis, physiological activity screening and analysis, writing, drafting and editing the manuscript, labelled the figures, tables and analyzed the data; Mohammad A. Iqbal synthesized and characterized the compounds; M. Asif conducted the Luciferase reporter gene assay; Tabinda A. conducted the synthesis of FLVM compound; Majid A. conducted the DPPH and Feric assay; Rosenani A. H. co-supervised the research; M. K. A. arranged the synthesis work with Dr Rose group and participated in objective preparation; Aman S. A. Majid co-supervised the research and developed the materials-methods; Amin. M. S. Abdul Majid editing the manuscript, planned the research objectives and supervised the research.

Acknowledgment

This research work was supported by EMAN Biodiscoveries Sdn Bhd funding, Universiti Sains Malaysia (USM) under the Research University Grant (RUT) [grant number 1001/PKIMIA/811217] and [grant number RUT 1001/PFARMASI/851001] and NKEA Research Grant Scheme (NRGS) number 304/CIPPT/650737/K123. Authors are thankful to the USM doctoral fellowship USM-APEX fellowship 2014-2015 grant # APEX(1002/JHEA/ATSG4001. We appreciate the spontaneous academic support of Prof. Roberta Fruttero and Prof. Barbara Rolando, University of Turin, Italy; Dr. Zulkifli Mustafa (Department of Neuroscience, University of Science Malaysia, School of Medicine); Dr. Michael M. Gottesman, M.D. (Laboratory of Cell Biology, National Cancer Institute, Bethesda, USA); Dr. Vikneswaran Murugaiyah, (Department of Pharmacology, University of Science Malaysia, School of Pharmaceutical Sciences); Dr. Siti Yusof, Mr. Mohammad Razak Hamdan and Dr. Zurina Hassan (Centre for Drug Research, School of Pharmaceutical Sciences, University of Science Malaysia).

Competing financial interests

The author(s) declare no competing financial interests.

References

ACD/Ilab2, version 12.01. (2015). Advanced Chemistry Development, Inc., (Toronto, ON, Canada), www.acdlabs.com.

Angelo LS, Kurzrock R. (2007). Vascular endothelial growth factor and its relationship to inflammatory mediators. *Clin Cancer Res.*, 13(10), 2825-30.
<https://doi.org/10.1158/1078-0432.CCR-06-2416>
PMid:17504979

Aldred, S.; Bennet, S.; Mecocci, P. (2010). Increased low-density lipoprotein oxidation, but not total plasma protein oxidation, in Alzheimer's disease. *Clinical Biochemistry*, 43, 267-271.
<https://doi.org/10.1016/j.clinbiochem.2009.08.021>
PMid:19733555

Bennet, S.; Grant, M. M.; Aldred, S. (2009). Oxidative Stress in Vascular Dementia and

Alzheimers Disease: A Common Pathology. *Journal of Alzheimer's Disease*, 17, 245-257.

Benzie IFF and Strain JJ. (1996). The ferric reducing ability of plasma (FRAP) as a measure
<https://doi.org/10.25163/angiotherapy.21206512012110519>

of 'antioxidant power': the FRAP assay. *Anal Biochem.*, 239, 70-76.

<https://doi.org/10.1006/abio.1996.0292>

PMid:8660627

Cancer Incidence in Peninsular Malaysia, Malaysian Natinal Cancer Council (MAKNA). (2006).

Dohle DS, Pasa SD, Gustmann S, Laub M, Wissler JH, Jennissen HP, Dünker N. (2009).

Chick ex ovo culture and ex ovo CAM assay: how it really works. *Journal of Visual Experiment*, 30(33), Pii, 1620.

<https://doi.org/10.3791/1620>

PMid:19949373 PMCID:PMC3157849

Douglas E. V. Pires, Tom L. Blundell, David B. (2015). Ascher, predicting small-molecule pharmacokinetic properties using graph-based signatures. *J. Med. Chem.*, 58 (9), 4066-4072.

<https://doi.org/10.1021/acs.jmedchem.5b00104>

PMid:25860834 PMCID:PMC4434528

Falé PL, Madeira PJ, Florêncio MH, Ascensão L, Serralheiro ML. (2011). Function of *Plectranthus barbatus* herbal tea as neuronal acetylcholinesterase inhibitor. *Food Funct.*, 2(2), 130-6.

<https://doi.org/10.1039/C0FO00070A>

PMid:21779558

Georgina N. Masoud, Wei Li. (2015). HIF-1 α pathway: role, regulation and intervention for cancer therapy, *Acta Pharmaceutica Sinica B*, 5(5):378-389

<https://doi.org/10.1016/j.apsb.2015.05.007>

PMid:26579469 PMCID:PMC4629436

Geran, R.I., Greenberg, N.H., Macdonald, M.M., Schumacher, A.M. and Abbott, B.J.

(1971). Protocols for screening chemical agents and natural products against animal tumours and other biological systems. *Canada Chemotherapy Report*, 12, 59-61.

Hayashi, T.; Shisido, N.; Nakayama, K.; Nunomura, A.; Smith, M. A.; Perry, G.; Nakamura, M. (2007). Lipid peroxidation and 4-hydroxy-2-nonenal formation by copper ion bound to
<https://doi.org/10.1016/j.freeradbiomed.2007.08.013>

PMid:17964426

amyloid- β peptide. *Free Radical Biology and Medicine*, 43, 1552-1559.

Hu J, Ye H, Zhang D, Liu W, Li M, Mao Y, Lu Y. (2013). U87 MG glioma cells overexpressing IL-17 accelerate early-stage growth in vivo and cause a higher level of CD31 mRNA expression in tumor tissues. *Oncol Lett.*, 6(4), 993-999.

<https://doi.org/10.3892/ol.2013.1518>

PMid:24137452 PMCID:PMC3796409

Jafari, S. F., Ahamed, K., Mohamed, B., Iqbal, M. A., Al Suede, F. S. R., Khalid, S. H., Haque, R. A., Nassar, Z. D., Umar, M. I. & Majid, A. (2014). Increased aqueous solubility and proapoptotic activity of potassium koetjapate against human colorectal cancer cells. *Journal of Pharmacy and Pharmacology.*, 66(10), 1394-1409.

<https://doi.org/10.1111/jphp.12272>

PMid:25039905

Khan Md Shamsuddin Sultan, Syeed Sharif Hossain, Uddin Md Hanif, Akter Lucky, Ullah Md

Asmat et al. (2013). Screening and evaluation of antioxidant, antimicrobial, cytotoxic,
E097-E122 | ANGIOTHERAPY | Published online May 11, 2019

- thrombolytic and membrane stabilizing properties of the methanolic extract and solvent-solvent partitioning effect of *Vitex negundo* Bark. *Asian Pac J Trop Dis.*, 3(5), 393-400.
[https://doi.org/10.1016/S2222-1808\(13\)60090-0](https://doi.org/10.1016/S2222-1808(13)60090-0)
- Khan Md Shamsuddin Sultan, Salam Md Abdus, Haque Rosenani S.M.A., Abdul Majid Amin Malik Shah, Abdul Majid Aman Shah Bin, Asif Muhammad, Basheer Mohamed Khadeer Ahamed, Tabana Yaseer M. (2016a). Synthesis, cytotoxicity, and long-term single dose anti-cancer pharmacological evaluation of dimethyltin(IV) complex of N(4)-methylthiosemicarbazone (having ONS donor ligand). *Cogent Biology*, 2, 1154282.
<https://doi.org/10.1080/23312025.2016.1154282>
- Khan MS, Majid AM, Iqbal MA, Majid AS, Al-Mansoub M, Haque RS. (2016b). Designing the angiogenic inhibitor for brain tumor via disruption of VEGF and IL17A expression. *Eur J Pharm Sci.*, 93, 304-18.
<https://doi.org/10.1016/j.ejps.2016.08.032>
PMid:27552907
- Kay F. Macleod. (2008). The role of the RB tumour suppressor pathway in oxidative stress responses in the haematopoietic system. *Nat Rev Cancer.* 8(10). 769-781.
<https://doi.org/10.1038/nrc2504>
PMid:18800074 PMCID:PMC2989879
- Kuzuya, M.; Yamada, K.; Hayashi, T.; Funaki, C.; Naito, M.; Asai, K.; Kuzuya, F. (1992). Role of lipoprotein-copper complex in copper-catalysed peroxidation of low-density lipoprotein. *Biochimica et Biophysica Acta*, 1123, 334-341.
[https://doi.org/10.1016/0005-2760\(92\)90015-N](https://doi.org/10.1016/0005-2760(92)90015-N)
- Lamaison, J. L., Petitjean-Freytet, C. and Carnat, A. (1991). Medicinal Lamiaceae with antioxidant properties, a potential source of rosmarinic acid. *Pharm. Acta. Helv.*, 66(7), 185-188
- LeadIT 2.1.9. (2015). BioSolveIT GmbH, St. Augustin, Germany.
- Mohan, S., Abdelwahab, S.I., Kamalidehghan, B., Syam, S., May, K.S., Harmal, N.S.M., Shafiqiyaz, N., Hadi, A.H.A., Hashim, N.M., Rahmani, M., Taha, M.M.E., Cheah, S.C., Zajmi, A. (2012). Involvement of NF- κ B and Bcl2/Bax signaling pathways in the apoptosis of MCF7 cells induced by a xanthone compound Pyranocycloartobiloxanthone A. *Phytomedicine*, 19, 1007-1015.
<https://doi.org/10.1016/j.phymed.2012.05.012>
PMid:22739412
- Matsuzawa A. and Ichijo H., (2008). Redox control of cell fate by MAP kinase: physiological roles of ASK1-MAP kinase pathway in stress signaling. *Biochimica et Biophysica Acta*, 1780(11), 1325-1336.
<https://doi.org/10.1016/j.bbagen.2007.12.011>
PMid:18206122
- Nevins JR. (2001). The Rb/E2F pathway and cancer. *Hum Mol Genet.*, 10(7), 699-703.
<https://doi.org/10.1093/hmg/10.7.699>
- Neckers, L., and Ivy, P. S., 2003. *Curr. Opin. Oncol.* 15. 419-424.
<https://doi.org/10.1097/00001622-200311000-00003>
PMid:14624223
- Nicosia R, Ottinetti A. (1990). Growth of microvessels in serum-free matrix culture of rat aorta: a quantitative assay of angiogenesis in vitro. *Lab Invest.*, 63, 115-122.
<https://doi.org/10.25163/angiotherapy.21206512012110519>
- Okoh V O, Garba N A , Penney R B , Das J, Deoraj A, Singh K P , Sarkar S, Felty Q, Yoo C, Jackson R M and Roy D. (2015). Redox signalling to nuclear regulatory proteins by reactive oxygen species contributes to oestrogen-induced growth of breast cancer cells. *British Journal of Cancer*, 112, 1687-1702.
<https://doi.org/10.1038/bjc.2014.586>
PMid:25965299 PMCID:PMC4430710
- Oztekin Algul, Alper Karabulut, Necmiye Canancankatan, Aysegul Gorur, Nehir Sucu and Ozden Vezir. (2012). Apoptotic and Anti-Angiogenic Effects of Benzimidazole Compounds: Relationship with Oxidative Stress Mediated Ischemia/Reperfusion Injury in Rat Hind Limb. *Antiinflamm Antiallergy Agents Med Chem.*, 11(3), 267-75.
<https://doi.org/10.2174/1871523011202030267>
PMid:23173574
- Patel, R. P.; Svistunenko, D.; Wilson, M. T.; Darley-Usmar, V. M. (1997). Reduction of Cu(II) by lipid hydroperoxides: implications for the copper-dependent oxidation of low density lipoprotein. *Biochemical Journal*, 322, 425-433.
<https://doi.org/10.1042/bj3220425>
PMid:9065759 PMCID:PMC1218208
- Pathi SS, Jutooru I, Chadalapaka G, Sreevalsan S, Anand S, Thatcher GR, and Safe S., (2011). GT-094, a NO-NSAID, inhibits colon cancer cell growth by activation of a reactive oxygen species-microRNA-27a: ZBTB10-specificity protein pathway. *Mol Cancer Res.* 9, 195-202.
<https://doi.org/10.1158/1541-7786.MCR-10-0363>
PMid:21156786 PMCID:PMC3069691
- Paladugu M, Thakur A, Lum LG, Mittal S, Parajuli P. (2013). Generation and immunologic functions of Th17 cells in malignant gliomas. *Cancer Immunol Immunother*, 62, 75-86.
<https://doi.org/10.1007/s00262-012-1312-7>
PMid:22752645 PMCID:PMC3888106
- Pratt, W. B., and Toft, D. O., (2003). Regulation of signaling protein function and trafficking by the hsp90/hsp70-based chaperone machinery. *Exp. Biol. Med.* 228, 111-133.
<https://doi.org/10.1177/153537020322800201>
- Polla BS, Kantengwa S, Francois D, Salvioli S, Franceschi C, Marsac C et al., (1996). Mitochondria are selective targets for the protective effects of heat shock against oxidative injury. *Proc Natl Acad Sci*, 93, 6458-6463.
<https://doi.org/10.1073/pnas.93.13.6458>
PMid:8692837 PMCID:PMC39045
- Petersen M., Abdullah Y., Benner J., Eberle D., Gehlen K., Hücherig S., Janiak V., Kim K. H., Sander M., Weitzel C., Wolters S. (2009). Evolution of rosmarinic acid biosynthesis.
<https://doi.org/10.1016/j.phytochem.2009.05.010>
PMid:19560175
- Phytochemistry, 70 (15-16), 1663-1679.
- Petersen M., Simmonds. M. S. (2003). Rosmarinic acid. *Phytochemistry*, 62(2), 121-125.
[https://doi.org/10.1016/S0031-9422\(02\)00513-7](https://doi.org/10.1016/S0031-9422(02)00513-7)
- Pinchuk, I.; Lichtenberg, D. (2002). The mechanism of action of antioxidants against lipoprotein peroxidation, evaluation based on kinetic experiments. *Progress in Lipid Research*, 41, 279- 314.
[https://doi.org/10.1016/S0163-7827\(01\)00026-1](https://doi.org/10.1016/S0163-7827(01)00026-1)

Scheckel KA, Degner SC, Romagnolo DF. (2008). Rosmarinic acid antagonizes activator protein-1-dependent activation of cyclooxygenase-2 expression in human cancer and nonmalignant cell lines. *J Nutr.*, 138(11), 2098-105.

<https://doi.org/10.3945/jn.108.090431>

PMid:18936204 PMCID:PMC3151436

Sharmila R, Manoharan S. (2012). Anti-tumor activity of rosmarinic acid in 7,12-dimethylbenz(a)anthracene (DMBA) induced skin carcinogenesis in Swiss albino mice. *Indian J Exp Biol.*, 50(3), 187-94.

Stupp R, Hegi ME, Mason WP, van den Bent MJ, Taphoorn MJ, Janzer RC et al. (2009). Effects of radiotherapy with concomitant and adjuvant temozolomide versus radiotherapy alone on survival in glioblastoma in a randomised phase III study: 5-year analysis of the EORTC-NCIC trial. *Lancet Oncol.*, 10(5), 459-66.

[https://doi.org/10.1016/S1470-2045\(09\)70025-7](https://doi.org/10.1016/S1470-2045(09)70025-7)

Syed, H. K., Iqbal, M. A., Haque, R. A. & Peh, K.-K. (2015). Synthesis, characterization and antibacterial activity of a curcumin-silver (I) complex. *Journal of Coordination Chemistry.*, 68(6), 1088-1100.

<https://doi.org/10.1080/00958972.2014.1003051>

Talley NJ, Zinsmeister AR, Weaver A, DiMagno EP, Carpenter HA, Perez-Perez GI, Blaser MJ. (1991). Gastric adenocarcinoma and *Helicobacter pylori* infection. *J Natl Cancer Inst.*, 83(23), 1734-9.

<https://doi.org/10.1093/jnci/83.23.1734>

PMid:1770552

Taub ME, Podila L, Ely D, Almeida I., (2005). Functional assessment of multiple P-glycoprotein (P-gp) probe substrates: influence of cell line and modulator concentration on P-gp activity. *Drug Metab Dispos.* 33 (11), 1679-87.

<https://doi.org/10.1124/dmd.105.005421>

PMid:16093365

Torres M. and Forman H. J., (2003). Redox signaling and the MAP kinase pathways. *BioFactors*, 17(1-4), 287-296.

<https://doi.org/10.1002/biof.5520170128>

Tuettenberg J, Friedel C, Vajkoczy P., (2006). Angiogenesis in malignant glioma-a target for antitumor therapy. *Crit Rev Oncol Hematol.* 59, 181-193

<https://doi.org/10.1016/j.critrevonc.2006.01.004>

PMid:16860996

Vikram Devgan, Abigail Harris, Qiong Jiang, and Scott Pattison. (2012). Signal Reporter Assay Kit: A high-performance tool for assessing the functions of genes, biologics, and small molecule compounds, QIAGEN, 6951 Executive Way, Frederick, Maryland 21703, USA.

Volkamer A, Kuhn D, Rippmann F, Rarey M. (2012). DoGSiteScorer: a web server for automatic binding site prediction, analysis and druggability assessment. *Bioinformatics.*, 28(15), 2074-5.

<https://doi.org/10.1093/bioinformatics/bts310>

PMid:22628523

Wainwright DA, Sengupta S, Han Y, Ulasov IV, Lesniak MS. (2010). The presence of IL-17A and T helper 17 cells in experimental mouse brain tumors and human glioma. *PLoS One* 2010, 5, e15390.

<https://doi.org/10.1371/journal.pone.0015390>

PMid:21060663 PMCID:PMC2963644

Wang, C., L. Wu, K. Bulek, B. N. Martin, J. A. Zepp, Z. Kang, C. Liu, et al., (2012). Psoriasis-associated variant Act1 D10N with impaired regulation by Hsp90. *Nature immunology.* 14 (1), 72-81.

<https://doi.org/10.1038/ni.2479>

PMid:23202271 PMCID:PMC3522792

Wang Q, Rager JD, Weinstein K, Kardos PS, Dobson GL, Li J, et al. (2005). Evaluation of the MDR-MDCK cell line as a permeability screen for the blood-brain barrier. *Int J Pharm.*, 288(2), 349-59.

<https://doi.org/10.1016/j.ijpharm.2004.10.007>

PMid:15620875

Zhang, Q. Ma Y, Cheng YF, Li WJ, Zhang Z, Chen SY., (2011). Involvement of reactive oxygen species in 2 methoxyestradiol-induced apoptosis in human neuroblastoma cells. *Cancer Lett.*, 31, 201-210.

<https://doi.org/10.1016/j.canlet.2011.09.005>

PMid:21978530 PMCID:PMC3224534

Zhou P, Sha H, Zhu J. (2010). The role of T-helper 17 (Th17) cells in patients with medulloblastoma. *J Int Med Res.* 38, 611-619.

<https://doi.org/10.1177/147323001003800223>

PMid:20515574

Submit your next manuscript to Journal of Angiotherapy published by EMAN Research

- Convenient online submission
- Thorough peer review
- No space constraints or color figure charges
- Immediate publication on acceptance
- Inclusion in Australian National Library and Google Scholar
- Both Open (80-100% subsidized APC by ER) & non-open access option

Submit your manuscript at
<https://angiotherapy.emanresearch.org>